








BRCA1/BARD1 intrinsically disordered regions facilitate chromatin recruitment and ubiquitylation

Samuel R Witus¹, Lisa M Tuttle^{1,†} , Wenjing Li^{2,†} , Alex Zelter¹ , Meiling Wang², Klaiten E Kermoade¹, Damien B Wilburn^{3,4}, Trisha N Davis¹ , Peter S Brzovic^{1,*} , Weixing Zhao^{2,**} , & Rachel E Klevit^{1,***} 

Abstract

BRCA1/BARD1 is a tumor suppressor E3 ubiquitin (Ub) ligase with roles in DNA damage repair and in transcriptional regulation. BRCA1/BARD1 RING domains interact with nucleosomes to facilitate mono-ubiquitylation of distinct residues on the C-terminal tail of histone H2A. These enzymatic domains constitute a small fraction of the heterodimer, raising the possibility of functional chromatin interactions involving other regions such as the BARD1 C-terminal domains that bind nucleosomes containing the DNA damage signal H2A K15-Ub and H4 K20me0, or portions of the expansive intrinsically disordered regions found in both subunits. Herein, we reveal novel interactions that support robust H2A ubiquitylation activity mediated through a high-affinity, intrinsically disordered DNA-binding region of BARD1. These interactions support BRCA1/BARD1 recruitment to chromatin and sites of DNA damage in cells and contribute to their survival. We also reveal distinct BRCA1/BARD1 complexes that depend on the presence of H2A K15-Ub, including a complex where a single BARD1 subunit spans adjacent nucleosome units. Our findings identify an extensive network of multivalent BARD1-nucleosome interactions that serve as a platform for BRCA1/BARD1-associated functions on chromatin.

Keywords BRCA1/BARD1; chromatin; DNA repair; intrinsically disordered region; ubiquitin

Subject Categories Chromatin, Transcription & Genomics; DNA Replication, Recombination & Repair; Post-translational Modifications & Proteolysis

DOI 10.15252/emboj.2023113565 | Received 19 January 2023 | Revised 10 April 2023 | Accepted 22 May 2023 | Published online 12 June 2023

The EMBO Journal (2023) 42: e113565

Introduction

Mutations in *BRCA1* and *BARD1* increase lifetime risk of breast and ovarian cancer. BRCA1 and BARD1 form a large, obligate

heterodimeric complex (BRCA1/BARD1) that has distinct roles in DNA double-stranded break (DSB) repair by homologous recombination (HR), transcriptional regulation, and several other nuclear processes (Mullan *et al*, 2006; Densham & Morris, 2019; Tarsounas & Sung, 2020). These functions are mediated, at least in part, through a direct association with chromatin. Upon DNA damage, BRCA1/BARD1 is recruited to damaged chromatin where it segregates with DNA repair factors (Scully *et al*, 1997; Kolas *et al*, 2007; Sobhian *et al*, 2007; Mattioli *et al*, 2012). Cancer-predisposing mutations that disrupt BRCA1/BARD1 functions on chromatin lead to DNA-damage hypersensitivity and genomic instability (Gudmundsdottir & Ashworth, 2006; Alenezi *et al*, 2020; Kraiss & Johnson, 2020). BRCA1/BARD1 also has distinct roles in both stimulation and repression of transcription through as yet incompletely defined mechanisms (Mullan *et al*, 2006). Full knowledge of how BRCA1/BARD1 interacts with chromatin and where it exerts its major biological functions are critical for understanding the etiology of BRCA1/BARD1-mutant-associated breast and ovarian cancer.

Nucleosomes, the organizing unit of chromatin, directly interact with BRCA1/BARD1 through multiple direct binding interfaces (Witus *et al*, 2022). The N-terminal RING domains of BRCA1 and BARD1 form a heterodimer that constitute a RING-type E3 ubiquitin (Ub) ligase and provide the only known enzymatic activity of BRCA1/BARD1 (Lorick *et al*, 1999; Brzovic *et al*, 2001; Witus *et al*, 2021b). The RING heterodimer binds to the histone surface of one pseudo-symmetrical “face” of a nucleosome to facilitate site-specific transfer of mono-Ub to a cluster of lysine residues on the extreme C-terminal tail of canonical histone H2A variants (K125, K127, and K129; henceforth referred to collectively as K127) (Kalb *et al*, 2014; Hu *et al*, 2021; Witus *et al*, 2021a). H2A lysine specificity is largely determined by the RING domain of BARD1. This domain binds to a unique histone surface compared to structurally similar Ub ligase complexes that target other H2A lysine residues (e.g., K119 by RING1B/BMI1) (McGinty *et al*, 2014). The H2A ubiquitylation (“H2A-Ub”) activity of BRCA1/BARD1 is thought to promote

¹ Department of Biochemistry, University of Washington, Seattle, WA, USA

² Department of Biochemistry and Structural Biology, University of Texas Health Science Center at San Antonio, San Antonio, TX, USA

³ Department of Genome Sciences, University of Washington, Seattle, WA, USA

⁴ Department of Chemistry and Biochemistry, The Ohio State University, Columbus, OH, USA

*Corresponding author. Tel: +1 (206) 685 1550; E-mail: brzovic@uw.edu

**Corresponding author. Tel: +1 (210) 450 5327; E-mail: zhaow2@uthscsa.edu

***Corresponding author. Tel: +1 (206) 543 5891; E-mail: klevit@uw.edu

[†]These authors contributed equally to this work

long-range resection of broken DNA ends during DSB repair via HR (Densham *et al*, 2016; Uckelmann *et al*, 2018). BRCA1/BARD1-dependent H2A-Ub activity is also implicated in the transcriptional repression of certain estrogen-metabolizing cytochrome P450 genes and the constitutive repression of α -satellite DNA regions (Zhu *et al*, 2011, 2018; Stewart *et al*, 2018; Thapa *et al*, 2022).

The BARD1 C-terminal domains (CTDs; Fig 1A) also bind to nucleosomes to facilitate DNA DSB repair (Nakamura *et al*, 2019; Becker *et al*, 2021; Dai *et al*, 2021; Hu *et al*, 2021; Kraiss *et al*, 2021; Sherker *et al*, 2021). The BARD1 CTDs specifically recognize nucleosomes that contain H2A K15-Ub (a product of the Ub E3 RNF168) and unmethylated H4 K20 (H4K20me0). Together, these signals serve as a binding platform for the recognition of damaged chromatin in S/G2 phases when a newly replicated sister chromatid is

available to template high-fidelity DNA repair via HR. The BARD1 CTDs and N-terminal BRCA1/BARD1 RING domains bind to histone surfaces that overlap, precluding their simultaneous binding to one nucleosome face. Despite this, mono-nucleosomes with ubiquitin preinstalled at both copies of H2A K15 residues are better substrates for BRCA1/BARD1-dependent ubiquitylation of H2A K127 *in vitro* (Hu *et al*, 2021). This observation implies that both domains may bind to the same nucleosome unit, with each occupying one face. Additionally, regions throughout the expansive intrinsically disordered segments of both BRCA1 and BARD1 are reported to bind to DNA, but the functional significance of such interactions in chromatin binding and H2A-Ub activity remains to be determined (Mark *et al*, 2005; Simons *et al*, 2006; Masuda *et al*, 2016; Zhao *et al*, 2017).

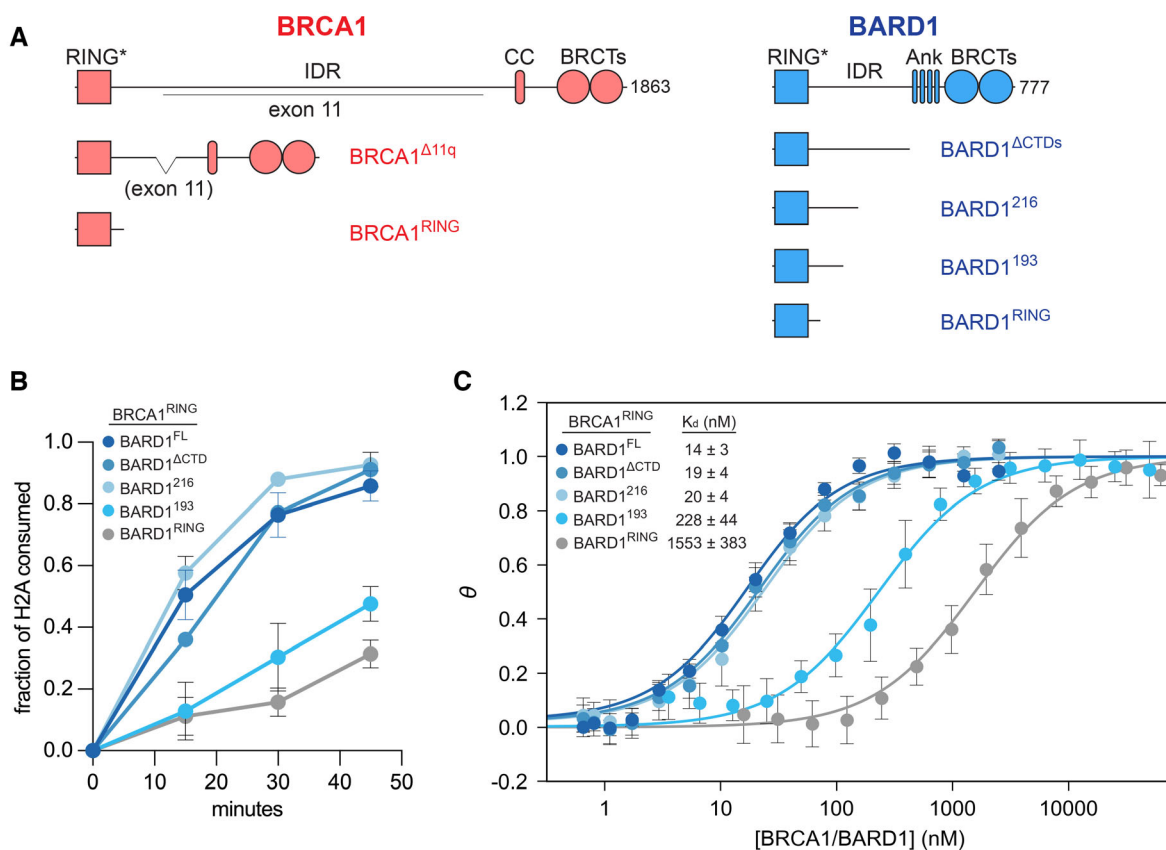


Figure 1. Contributions of BARD1 regions to nucleosome binding and H2A-Ub activity.

A Domain organization of BRCA1 and BARD1. The domain names are indicated above the cartoons (RING, really interesting new gene; IDR, intrinsically disordered region; CC, coiled coil; BRCT, BRCA1 C-terminal; Ank, Ankyrin repeat domain; CTD, C-terminal domain). Constructs used to generate data in panels (B and C) are shown; residue bounds are reported in Appendix Table S1.

B Quantification of time-course nucleosome H2A-Ub assays using the indicated BRCA1/BARD1 truncations. Data are presented as the normalized fraction of H2A consumed during a time-course nucleosome ubiquitylation assay. Data points represent mean values and error bars are ± 1 -s.d. of $n = 3$ independent technical replicate experiments. The residue bounds of BRCA1^{RING} are 1–112, and BARD1^{RING} are 26–140. A comprehensive list of residue bounds can be found in Appendix Table S1. Additional details about all reagents used in these studies can be found in the methods section. Representative gels of assays that are quantified in this panel are shown in Fig EV1A.

C Nucleosome binding curves from fluorescence-quenching-based measurements using the indicated BRCA1/BARD1 constructs. Data show mean values and error bars are ± 1 -s.d. of $n = 4$ independent technical replicate experiments. The reported difference in affinities to BRCA1^{RING}/BARD1^{RING} is likely underestimated, as the minimal RING/RING heterodimer binding data was collected at a lower ionic strength than the other constructs to obtain well-behaved binding data (50 mM vs. 100 mM NaCl).

Source data are available online for this figure.

Although a minimal RING/RING heterodimer is sufficient to direct the transfer of mono-Ub to H2A K127 in nucleosomes, full-length BRCA1/BARD1 heterodimers form stronger complexes with unmodified nucleosome substrates and exhibit increased H2A-Ub activity (Hu *et al*, 2021; Witus *et al*, 2021a). This suggests that additional interactions between full-length BRCA1/BARD1 and nucleosomes can occur in the absence of the DNA-damage-specific H2A K15-Ub histone marks. Because BRCA1/BARD1 performs diverse biological functions in the nucleus including, but not limited to, DNA repair via HR, transcriptional regulation, stalled replication fork protection, centrosome regulation, R-loop resolution, and cell-cycle regulation, it is likely that the complex can be recruited to chromatin via signals not limited to H2A K15-Ub. In pursuit of a wholistic understanding of BRCA1/BARD1 recruitment to chromatin, we sought to characterize interactions with nucleosomes that lead to enhanced chromatin binding and H2A-Ub activity in both the absence and presence of H2A K15-Ub marks.

Here, we identify an intrinsically disordered region of BARD1 adjacent to its RING domain that binds strongly to both nucleosomal and extra-nucleosomal DNA, dramatically enhancing the affinity of the complex and its H2A-Ub activity. The interactions can be modulated by specialized DNA structures that are derived from the DNA damage repair process and can compete directly with BARD1 binding to nucleosomal DNA. We incorporate our findings into a molecular mechanism of recognition and establish a role for BARD1–DNA interactions in chromatin recruitment and DNA damage repair in cells. Additionally, we provide evidence for multiple, distinct higher order chromatin complexes that contain H2A K15-Ub nucleosomes. These include both a “wrapped” complex with the BRCA1/BARD1 RING domains and BARD1 CTDs bound to opposite sides of one nucleosome unit, as well as an extended complex where the domains bind to adjacent nucleosome units. Throughout, we evaluate the contribution of BARD1 DNA binding to nucleosome affinity and H2A-Ub activity. Our findings reveal a network of multivalent BARD1–nucleosome interactions that serve as a platform for BRCA1/BARD1-associated functions on chromatin and hint at novel modes of DNA recognition by intrinsically disordered regions of proteins.

Results

BARD1 IDR supports increased H2A ubiquitylation activity

The BRCA1/BARD1 heterodimer contains both structured domains and long intrinsically disordered regions (IDRs; Fig 1A). A minimal complex composed of the N-terminal RINGs of BRCA1 (1–112) and BARD1 (26–140; BRCA1^{RING}/BARD1^{RING}) is sufficient to direct site-specific mono-ubiquitylation of nucleosomal histone H2A at K127 (Kalb *et al*, 2014). We and others have observed that full-length BRCA1/BARD1 (~300 kDa) exhibits faster H2A-Ub kinetics and stronger binding to unmodified mono-nucleosomes than the minimal RING/RING complex (~25 kDa; Fig EV1A–D) (Hu *et al*, 2021; Witus *et al*, 2021a). To identify regions responsible for increased H2A-Ub activity and binding affinity, we generated heterodimers with truncations in either BRCA1 or BARD1 (Appendix Fig S1 and Appendix Table S1).

Heterodimers containing full-length BARD1 and three BRCA1 constructs were compared to survey BRCA1 regions that may

enhance H2A-Ub activity: full-length BRCA1 (BRCA1^{FL}), a clinically relevant allele missing ~1,100 residues in the expansive IDR (BRCA1^{Δ11q}), and the minimal BRCA1 RING fragment (BRCA1^{RING}). Notably, in the context of BARD1^{FL}, the RING domain of BRCA1 is sufficient to generate fast H2A-Ub kinetics (Fig EV1C). The presence of additional regions of BRCA1 either do not further enhance activity (as in BRCA1^{Δ11q}/BARD1^{FL}) or appear to inhibit activity (e.g., BRCA1^{FL}/BARD1^{FL}). These results indicate that the BARD1 subunit is largely responsible for enhanced H2A-Ub activity. In the context of heterodimers that contain only the RING of BARD1, modest activity enhancements are afforded by inclusion of additional BRCA1 regions, suggesting that, in the absence of FL-BARD1, regions of BRCA1 may provide some redundancy in function (Fig EV1D).

To identify regions of BARD1 that contribute to increased H2A-Ub activity, the H2A-Ub kinetics and nucleosome-binding affinity of BRCA1^{RING}-heterodimers containing BARD1 truncations were compared. Notably, BRCA1^{RING}/BARD1^{FL} heterodimers bind nucleosomes with ~100-fold higher affinity than minimal BRCA1^{RING}/BARD1^{RING} and have markedly higher H2A-Ub activity (Fig 1B and C). Removal of the BARD1 C-terminal domains (BARD1^{ΔCTD}) or truncation back to residue 216 in the putative intrinsically disordered region (BARD1²¹⁶) had minimal impact on H2A-Ub activity and nucleosome binding (Fig 1B and C). However, truncation to residue 193 (BARD1¹⁹³) caused a substantial decrease in H2A-Ub activity and a >10-fold reduction in binding affinity, suggesting a nucleosome-binding interface for residues between 194 and 216. Consistent with this, deletion of the first half of the BARD1 IDR (BARD1^{Δ140–270}) greatly diminished H2A-Ub activity (Fig EV1E). Although deletion of residues 140–270 decreased nucleosome-binding affinity by ~3-fold relative to full-length BARD1, the affinity is still considerably stronger than the minimal RING/RING heterodimer or BARD1¹⁹³ truncations (Fig EV1F). A more targeted deletion (BARD1^{Δ194–216}) only modestly decreased H2A-Ub activity, suggesting the presence of additional or compensatory nucleosome interaction sites in BARD1 *in vitro*. Intrinsic nucleosome-binding properties of BARD1 IDRs were analyzed using constructs containing only the N-terminal half (residues 124–270) or only the C-terminal half (residues 269–424). Each IDR-only construct exhibited nucleosome binding by EMSA, with modest differences in affinity (Fig EV1G). This is consistent with the highly basic nature of both halves of the BARD1 IDR (pI > 9; Wilkins *et al*, 1999). In summary, only the RING domain of BRCA1 is required for high H2A-Ub activity *in vitro* while a small region within the BARD1 IDR (BARD1 141–216, referred to in the discussion as IDR^{Prox}) that engages in nucleosome binding is required in addition to the BARD1 RING to support increased H2A-Ub activity.

Characterization of the BARD1 IDR reveals that the additional BARD1–nucleosome interactions are mediated through DNA binding

BARD1 residues 141–216 identified as contributing to increased H2A-Ub activity and nucleosome binding are in the large central segment predicted to be intrinsically disordered (124–424) (McGuffin *et al*, 2000). Nuclear magnetic resonance (NMR) ¹H¹⁵N-HSQC spectra of ¹⁵N-BARD1 fragments containing residues 124–270, 269–424, and 124–424 each exhibited narrow ¹H chemical shift dispersion consistent with intrinsic disorder (Fig EV2A and B).

Furthermore, individual spectra of BARD1 IDRs 124–270 and 269–424 overlay well with the spectrum of the full region (124–424), indicating that the two regions behave independently of one another (Fig EV2B).

Despite being intrinsically disordered, the BARD1 124–270 sequence is largely conserved across orthologs (Fig EV2C). The region was previously reported to bind to double-stranded DNA and specialized DNA structures containing base-pair mismatch (discussed below) (Zhao *et al*, 2017). Notably, the amino acid composition in this region contains several conserved clusters of basic residues that are not observed elsewhere in the BARD1 IDR (Fig EV2C, Appendix Fig S2). We therefore hypothesized that the contributions of the BARD1 IDR (residues 141–216) to increased binding and activity are mediated through interactions with nucleosomal DNA. Indeed, BARD1 124–270 binds strongly to nucleosomes and to free 147-bp “601” dsDNA by EMSA (Fig EV3A).

For residue-level information, we performed NMR-binding experiments with ^{15}N -labeled BARD1 124–270 and either a 36-bp dsDNA fragment or mono-nucleosomes wrapped with 147-bp dsDNA (Figs 2A and EV3B). Experimentally, a full titration was possible only with the dsDNA fragment due to its lower molecular weight and higher solubility. The spectral series displayed a subset of

resonances that shift continuously as a function of DNA concentration (Fig 2A). A similar set of resonances was perturbed (broadened in this case) upon addition of 147-bp nucleosome, indicating that similar BARD1 residues engage nucleosomes and free dsDNA (Fig EV3B). To overcome spectral overlap in the spectrum of BARD1 124–270, the spectrum of a smaller construct containing the putative DNA-binding region (BARD1 141–216, where residue 141 is the first to extend beyond BARD1^{RING}) was assigned, and assignments were transferred to the longer segment, enabling analysis in both contexts (Figs 2A and B, and EV3B and C). Secondary structure propensity (SSP) predicted from the resonance assignments are consistent with the region being primarily disordered, with some modest helical propensity predicted for residues 191–201 and a weaker prediction of extended structure near the beginning of the construct (Fig EV3E). The values are consistent with these regions populating secondary structures at a low population or that the secondary structure is highly dynamic.

BARD1 residues 194–216 exhibit the largest backbone amide chemical shift perturbations (CSPs) due to dsDNA addition, with smaller perturbations observed for residues 146–161 (Fig 2B). Residues between 162–191 were relatively unaffected by dsDNA, consistent with the existence of distinct DNA-binding regions within the

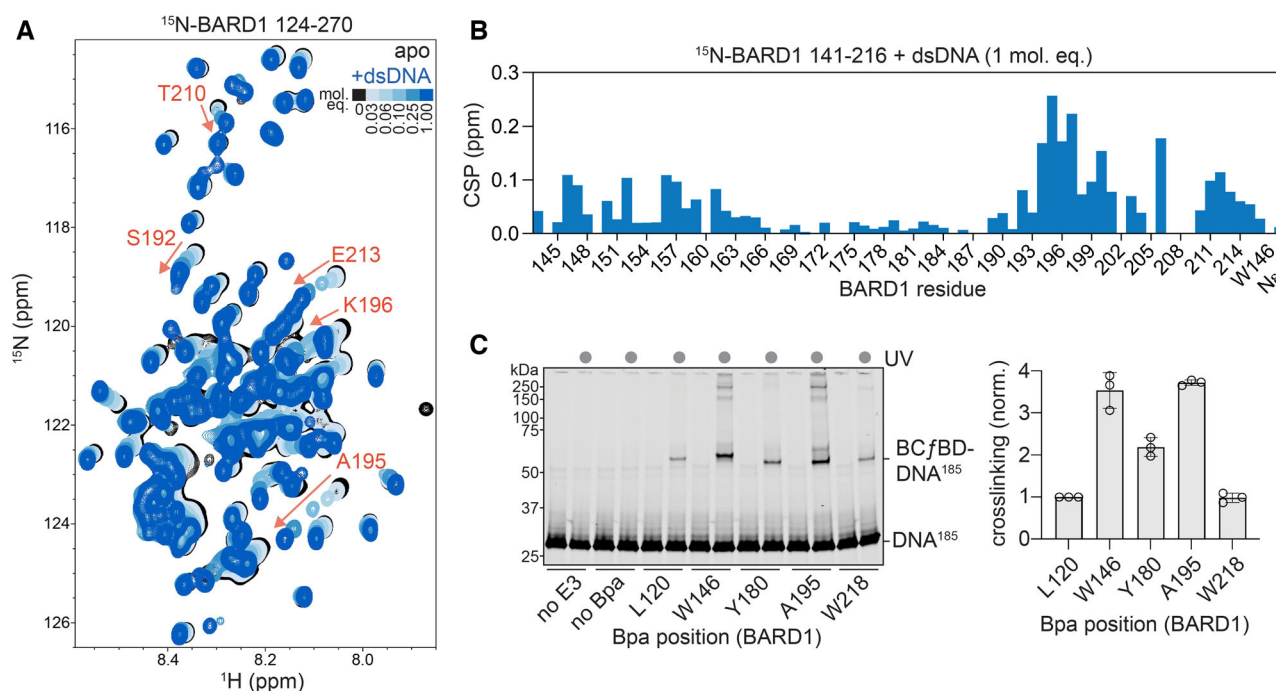


Figure 2. The BARD1 IDR binds to nucleosomes via DNA.

- A ^1H - ^{15}N -HSQC NMR titration of ^{15}N -BARD1 124–270 with a 36-bp dsDNA fragment. Darker shades of blue correspond to increasing amounts of DNA added. A subset of highly affected signals is labeled with their residue identities, with arrows showing their trajectories over the course of the titration.
- B ^1H - ^{15}N -HSQC NMR amide chemical shift perturbations (CSPs) observed for ^{15}N -BARD1 141–216 signals when bound to a 36-bp dsDNA fragment (1:1 molar equivalent complex).
- C Representative SDS-PAGE gel monitoring in-gel fluorescence (labeled DNA) of UV-induced Bpa cross-linking of the E3 ligase fusion BRCA1^{1–104}-f-BARD1²²¹ (BCfBD) to nucleosomes (left). In this construct, the C-terminus of BRCA1^{1–104} is genetically fused to the N-terminus of BARD1^{26–221} via a 12-residue GlySer-linker. Quantification of Bpa cross-linking experiments with nucleosomes (right). The intensity of each cross-linked band was normalized to the intensity of the L120Bpa cross-linked band for each replicate experiment. Graph bars show the mean; error bars are ± 1 -s.d. and the open circles are the values of individual replicates for of $n = 3$ independent technical replicate experiments.

Source data are available online for this figure.

IDR. Secondary structure predicted from chemical shifts in the presence of dsDNA (1 molar equivalent) indicate a reduction in helical propensity in residues 191–199 upon DNA binding (Fig EV3E). A reduction in helical propensity upon DNA-binding contrasts with many IDR regions that gain secondary structure upon binding to their targets (Davey, 2019). As well, ^{15}N dynamics measurements reveal that residues 146–161 undergo changes in dynamics in the presence of dsDNA (Fig EV3F). Although low solubility limited similar analysis on nucleosome-bound samples, the similar spectral perturbations observed in the presence of low molar equivalents of nucleosomes or dsDNA suggest similar protein-DNA-binding modes (Fig EV3B). Thus, the data reveal two IDR regions adjacent to the RING domain (146–161 and 194–216) that bind DNA when presented as free dsDNA or in the context of a nucleosome. These regions are consistent with the H2A-Ub activity and nucleosome-binding results presented above.

Having established that isolated BARD1 IDR fragments bind to nucleosomes, we sought to observe the interactions within the context of an active enzymatic complex. As such a complex is too large for NMR analysis using conventional isotopic labeling and data collection schemes, we employed targeted cross-linking of BRCA1/BARD1 to nucleosomal DNA. Photoactivatable cross-linker p-benzoyl-L-phenylalanine (Bpa) was incorporated at individual positions in the BARD1 IDR in the context of RING-containing constructs using amber-codon suppression in *Escherichia coli* (L120Bpa, W146Bpa, Y180Bpa, A195Bpa, and W218Bpa; Appendix Fig S3A). Due to the need to co-express a Bpa-specific aminoacyl tRNA transferase, we designed a genetic fusion in which BRCA1 residues 1–104 are fused to BARD1 residues 26–221 through a 12-residue GlySer-linker (BRCA1-*f*-BARD1²²¹). Wild-type BRCA1-*f*-BARD1²²¹ and Bpa-incorporated mutants retained similar H2A-Ub activity to each other and to unfused heterodimers (Appendix Fig S3B). Nucleosomes with extra-nucleosomal linker DNA that carried a fluorescent probe enabled visualization of covalent BARD1-DNA cross-linked products

via SDS-PAGE (NCP¹⁸⁵; Appendix Fig S3C). Such bands were detected for every Bpa variant, with enhanced cross-linking by variants with Bpa at BARD1 W146 and A195 positions, consistent with the NMR dsDNA-binding data presented above (Fig 2C). Cross-linked bands were weaker from Y180 and W218 positions and comparable to cross-links from L120, which is located close to the RING domains and not expected to contribute to productive DNA interactions. A similar pattern was observed in cross-linking reactions containing free DNA (Appendix Fig S3D). As cross-links can only form from Bpa to sites that are within $\sim 3 \text{ \AA}$, the data support a direct interaction between the BARD1 IDR and nucleosomal DNA in the context of an enzymatically active complex.

Contribution of DNA binding to enhanced H2A-Ub activity

Results presented thus far establish that the DNA-binding region of the BARD1 IDR is necessary for high H2A-Ub activity, but is it sufficient? To address this question, we asked whether the DNA-binding properties of full-length BARD1 can support H2A-Ub activity in the presence of BARD1 RING mutations that disrupt the histone-binding interface (BARD1 P89A/W91A; Fig 3A) (Hu et al, 2021; Witus et al, 2021a). Heterodimers containing BRCA1^{RING} and full-length BARD1 (P89A/W91A) retain high-affinity nucleosome binding and auto-ubiquitylation activity but do not transfer Ub to H2A or any other histone sites (Fig 3B, Appendix Fig S4A–C). Thus, the BARD1 RING–histone interface is absolutely required for H2A-Ub activity, while the BARD1 IDR-DNA interactions promote formation of a high-affinity complex that supports enhanced H2A-Ub activity.

The BARD1 DNA-binding region(s) are disordered. To test whether any DNA-binding region placed adjacent to the RING domain can serve the same purpose, we created a chimeric BARD1 construct in which a previously identified DNA-binding region from the BRCA1 IDR (498–663) was appended onto the BARD1 RING

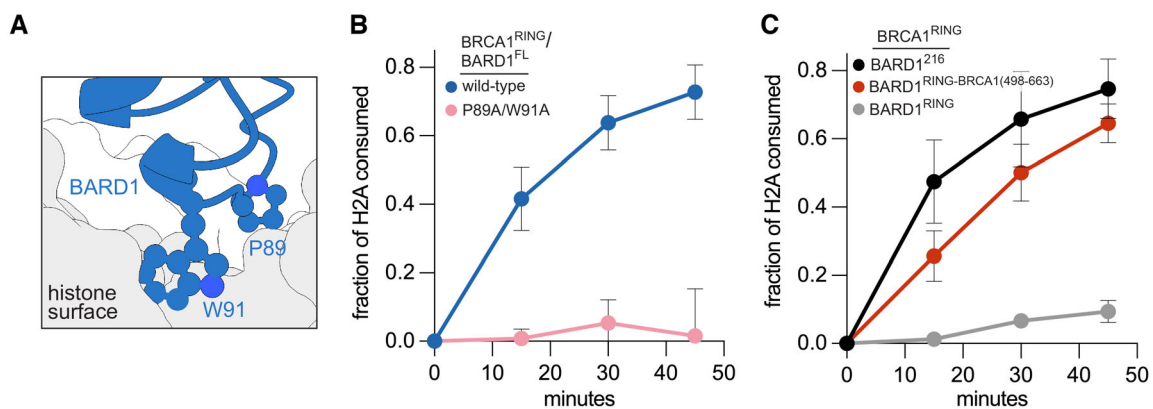


Figure 3. Contribution of BARD1 DNA binding and RING-histone binding to H2A-Ub activity.

A The BARD1 RING-histone interface showing the locations of BARD1 P89 and W91 relative to the histone surface, which is colored as a gray surface (PDB: 7JZV).
 B, C Quantification of H2A-Ub time-course assays using the indicated BRCA1/BARD1 constructs. Data show the mean; error bars are ± 1 -s.d. of $n = 3$ independent technical replicate experiments. Two single time-points from panel C from the BRCA1^{RING}/BARD1^{RING} curve were excluded from analysis due to their extremely low activities coupled with quenching/loading errors yielding normalized fraction of H2A consumed values of < 0 . Values for these excluded points are included as source data.

Source data are available online for this figure.

(Mark *et al.*, 2005). A heterodimer composed of BRCA1^{RING} and the BARD1 chimera displayed increased H2A-Ub activity compared to the minimal RING/RING complex, but not to the level of the native BARD1 sequence (Fig 3C). The nucleosome-binding affinities for these species are quite similar, suggesting that the modest activity difference between the native BARD1 region and the installed BRCA1-derived region arises from additional features (Appendix Fig S4D). The findings indicate that a major contributor to increased H2A-Ub activity is the presence of a disordered, high-affinity DNA-binding region near the enzymatic RING domains, but indicate that the BARD1 IDR is especially effective.

Specialized DNA structures bind to the BARD1 IDR and inhibit H2A-Ub activity

Based on a previous report that the BARD1 IDR preferentially binds to partly unwound DNA structures (bubble-DNA) and homologous recombination (HR) intermediates (D-loop DNA) over double- or single-stranded DNA (Zhao *et al.*, 2017), we hypothesized that interaction of the BARD1 DNA-binding region with bubble- or D-loop DNA might affect its ability to interact with nucleosomal DNA. Recognition modes of bubble- and D-loop-DNA substrates by BARD1 are likely similar based on the near-identical affinities of the BARD1-DNA complexes (Zhao *et al.*, 2017), so we used the simpler bubble-DNA substrate in our assays. In nucleosome ubiquitylation reactions carried out with full-length BRCA1/BARD1 in the presence of equal concentrations of DNA fragments containing various patterns of base-pair mismatch, only bubble-DNA substantially inhibited H2A-Ub activity (Fig 4A and B, Appendix Fig S5A and B). The minimal RING heterodimer activity was unaffected by bubble-DNA, consistent with the inhibition being due to competing interactions of bubble- and nucleosomal DNA for binding to BARD1 141–216 (Appendix Fig S5C and D). BARD1-nucleosome DNA cross-link formation was inhibited by either bubble-DNA or dsDNA in a concentration-dependent manner, with bubble-DNA being substantially more effective (Fig 4C, Appendix Fig S5E).

We compared the interactions of BARD1 141–216 with bubble- and dsDNA by NMR using DNA species of similar sequence and size. CSPs and changes in dynamics were similar within BARD1 194–216, the region identified as the major site for dsDNA and nucleosomal DNA binding (Figs 4D and EV3C, D and F). Much stronger effects were produced by bubble-DNA on backbone resonances of residues 143–157 with severe peak broadening/disappearance, indicative of large changes in chemical environment and/or dynamics. Only in the presence of bubble-DNA was a large CSP observed for the side-chain resonance of W146 (Figs 4D and EV3C and D). Additional effects on sidechains were observed in ¹H¹³C-HSQC spectra of BARD1 141–216 bound to bubble-DNA, where methyl group peaks from BARD1 residues 143–157 exhibit large CSPs that are not observed in the presence of dsDNA (Fig 4E, Appendix Fig S6). Together, the data show that bubble-DNA engages strongly and specifically at a site near the beginning of the BARD1 IDR (residues 143–157) and that both forms of DNA engage BARD1 194–216. To interrogate the functions of the DNA-binding regions, we made minimalist deletions in the BARD1 IDR that remove stretches of basic residues within both the general DNA-binding site (Δ 194–216) and the bubble-DNA-specific region (Δ 150–155). In agreement with our NMR data, both IDR regions appear to be functionally important, as

only concomitant deletion of basic residues in both IDR regions (BARD1 ^{Δ 150–155/ Δ 194–216}) fully alleviated H2A-Ub activity inhibition by bubble-DNA (Fig 4F, Appendix Fig S5F).

DNA-binding IDR facilitates chromatin recruitment and DNA damage repair in cells

To test the importance of BARD1 IDR DNA binding in a cellular context, we established doxycycline-inducible HeLa cell lines that deplete endogenous BARD1 via doxycycline-induced expression of shRNA against BARD1 (HeLa-shBARD1) and stably re-express shBARD1-resistant HA-tagged BARD1 (wild-type or Δ 194–216; Fig EV4A). Endogenous BARD1 is largely depleted (> 90%) in these cells and expression of wild-type BARD1 or BARD1 ^{Δ 194–216} stabilizes endogenous BRCA1. Wild-type BARD1 or BARD1 ^{Δ 194–216} each localize to the nucleus and are expressed at similar levels (Fig EV4A and B). In cellular fractionation assays, less BARD1 ^{Δ 194–216} is associated with chromatin than wild-type BARD1 under both basal and olaparib-induced DNA-damage conditions, as shown by a reduction in the ratio of BARD1 to histone H3 (Fig 5A). By microscopy, significantly reduced HA-BARD1 ^{Δ 194–216} foci formation was observed in both untreated and olaparib-induced DNA-damage conditions (Figs 5B and EV4C). This indicates a defect in BRCA1/BARD1 recruitment to chromatin and DNA damage sites. To assess the ability of the BARD1 IDR mutant to facilitate DNA break repair, we performed clonogenic survival assays upon treatment with DNA-damaging agents olaparib and cisplatin (Figs 5C and EV4D). Survival of BARD1 ^{Δ 194–216} cells was significantly reduced compared to wild-type controls under both drug treatments—a hallmark of defective HR (Fig 5C). Altogether, the results demonstrate that the short intrinsically disordered stretch of BARD1 with DNA-binding ability contributes to chromatin association in cells under both basal and exogenous DNA-damage conditions and contributes to DNA break repair required for cell survival.

Extra-nucleosomal linker DNA enhances H2A ubiquitylation

Chromatin is composed of adjacent nucleosome units separated by linker DNA. The extended domain topology of both BRCA1 and BARD1 with their long IDRs raises the possibility of interactions in higher-order chromatin substrates that are not present in minimal mono-nucleosome substrates. Nucleosome substrates with extra-nucleosomal linker DNA (NCP¹⁸⁵) and tri-nucleosomes (tri-NCP) were used as substrates in H2A-Ub assays to test for additional chromatin involvement (Fig 6A, Appendix Fig S7A). In reactions using full-length BRCA1/BARD1, faster H2A-Ub kinetics were observed for NCP¹⁸⁵ with linker DNA compared to the minimal NCP¹⁴⁷ substrate (Fig 6B). Notably, no additional increase in H2A-Ub activity was observed for a tri-NCP substrate despite containing a longer linker DNA and multiple histone-binding interfaces. The data are consistent with two conclusions: (i) the presence of linker DNA enhances BRCA1/BARD1 H2A-Ub activity and (ii) functional interactions are limited to one mono-nucleosome unit, at least in the absence of histone PTMs.

To explicitly test the BARD1 IDR DNA-binding region as the source of the enhanced activity observed for NCP¹⁸⁵ and tri-NCP substrates, the H2A-Ub activity of the BRCA1^{RING}/BARD1²¹⁶ truncation was tested (Fig 6C). This species exhibited considerably faster H2A-Ub kinetics with either NCP¹⁸⁵ or tri-NCP compared to a

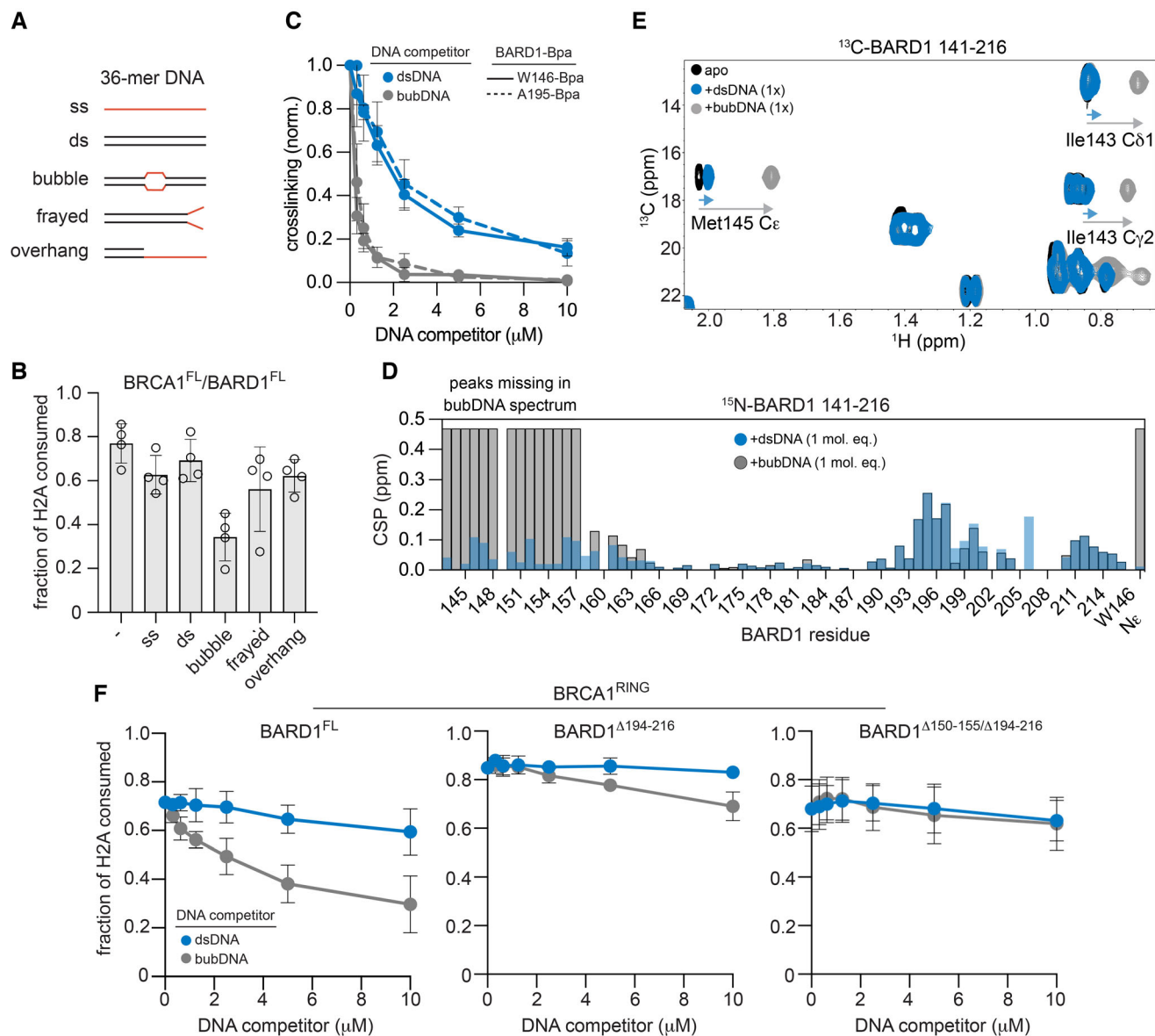


Figure 4. Inhibition of nucleosome binding and H2A-Ub by specialized DNA structures.

- A Design of 36-mer DNA competitor fragments used in H2A-Ub activity, Bpa cross-linking, and NMR assays. Red indicates non-base-paired regions. The number of unpaired bases or base-pairs is: ss – 36; ds – 0; bubble – 8; frayed – 8; ssOverhang – 24.
- B Single time-point H2A-Ub inhibition assays using BRCA1^{FL}/BARD1^{FL} (100 nM) and the indicated competitor DNA (2.5 μ M). Data show the mean; error bars are \pm 1-s.d.; and open circles are individual data points of $n = 4$ independent technical replicate experiments.
- C Inhibition of UV-induced Bpa cross-linking between the indicated BRCA1-f-BARD1²²¹ Bpa-incorporated constructs and NCP¹⁸⁵ substrates in the presence of increasing amounts of dsDNA or bubble-DNA competitor. Data show the mean; error bars are \pm 1-s.d. of $n = 3$ (W146Bpa) or $n = 4$ (A195Bpa) independent technical replicate experiments.
- D ¹H¹⁵N-HSQC NMR CSPs observed to ¹⁵N-BARD1 141–216 signals when bound to a 36-mer dsDNA (blue bars) or bubble-DNA (gray bars with black outlines) fragment (1:1 molar equivalent complex). Signals for residues 143–157 are broadened beyond detection in the bubble-DNA-bound spectrum; for visualization purposes, gray bars are set equal to the CSP value for the W146Ne CSP that was observed; the real CSP values are likely larger than this value (see Fig EV3C and D for corresponding spectra).
- E Selected region of ¹³C-HSQC spectra of ¹³C-BARD1 141–216 in 1:1 molar equivalent complex with dsDNA fragment (blue) or bubble-DNA fragment (gray). Signal trajectories in bound spectra are indicated by correspondingly colored arrows.
- F Single time-point H2A-Ub inhibition assays using heterodimers containing BRCA1^{RING}/BARD1^{FL} (left, 12 min endpoint) or the indicated BARD1 internal deletion mutant (middle and right, 20 min endpoint) and increasing amounts of dsDNA or bubble-DNA competitor. The same E3 concentration (50 nM) was used for each BRCA1/BARD1 truncation. A longer time point was used for the double-deletion mutant as the intrinsic H2A-Ub activity of this mutant was lower, likely due to the deletion of DNA-binding regions. Representative assay gels are shown in Appendix Fig S5F. Data show the mean; error bars are \pm 1-s.d. of $n = 3$ independent technical replicate experiments.

Source data are available online for this figure.

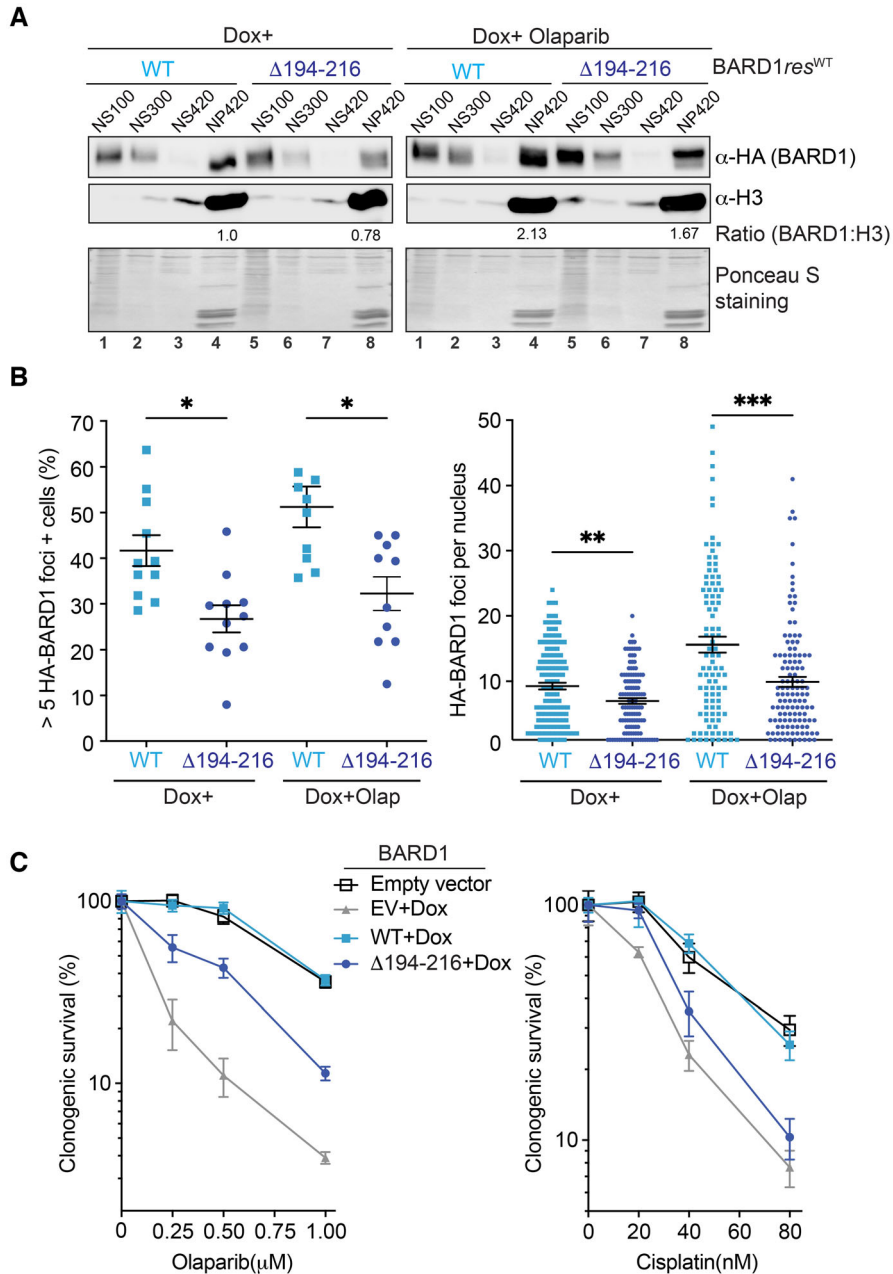


Figure 5. Cellular role for BARD1 DNA binding in chromatin recruitment and DNA damage repair.

A Western blot analysis to detect HA-BARD1 in nuclei isolated from HeLa-shBARD1 cells stably expressing wild-type or $\Delta 194-216$ mutant of HA-BARD1, where endogenous BARD1 was depleted by doxycycline-induced shBARD1 expression. The nuclei were salt-fractionated into NS100, NS300, NS420, and NP420 to assess the amount of HA-BARD1 associated with chromatin. Data are representative of $n = 2$ biological replicate experiments.

B Quantification of cells with > 5 HA-BARD1 foci (left panel) and number of HA-BARD1 foci per nucleus (right panel) with and without olaparib treatment. * $P < 0.05$, ** $P < 0.01$, *** $P < 0.001$, by Student's t -test. Data show the individual points from $n = 3$ biological replicate experiments.

C Clonogenic survival of HeLa-shBARD1 cells stably expressing wild-type or $\Delta 194-216$ mutant of HA-BARD1 upon treatment with indicated amount of olaparib and cisplatin. Data points show the mean; error bars represent s.e.m. of $n = 3$ biological replicate experiments.

Source data are available online for this figure.

minimal NCP¹⁴⁷ substrate, confirming that the dependence on linker DNA arises from the BARD1 IDR. The presence of linker DNA provides less than a twofold increase in binding affinity for BRCA1^{RING}/BARD1²¹⁶ to nucleosome core particles (NCPs) under buffer ionic-

strength conditions used in H2A ubiquitylation assays (Fig EV5A). Thus, in the absence of linker DNA, BARD1 IDR can interact nearly as well with nucleosomal DNA, but the interaction with linker DNA supports enhanced activity.

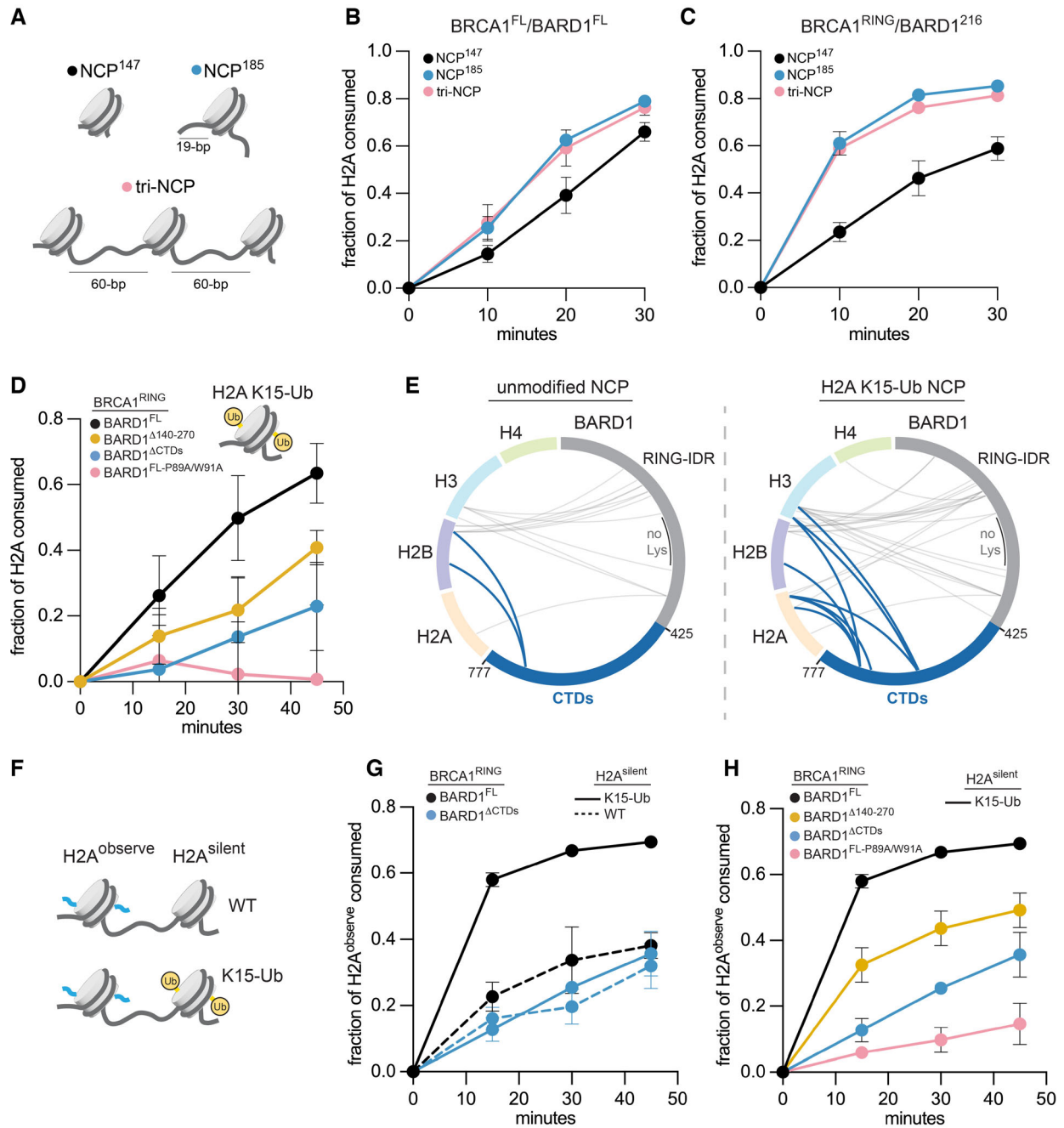


Figure 6. H2A-Ub activity using chromatin substrates with linker DNA and preinstalled H2A K15-Ub.

A Schematic of chromatin substrates used for H2A-Ub activity and nucleosome binding assays in panels B and C. The length of linker-DNA is indicated next to the NCP¹⁸⁵ and tri-NCP.

B, C Quantification of time-course H2A-Ub assays using the indicated BRCA1/BARD1 constructs and chromatin substrates.

D Quantification of time-course H2A-Ub assays using homogeneously modified H2A K15-Ub mono-nucleosome substrates and indicated BRCA1/BARD1 constructs.

E Intermolecular cross-links observed by chemical cross-linking and MS analysis between BARD1 and histones using wild-type (left) and H2A K15-Ub (right) 147-bp “601” nucleosomes and BRCA1^{RING}/BARD1^{FL} heterodimers. Cross-links to histones emanating from the CTDs of BARD1 are shown in blue, and the RING-IDR region in gray. A lysine-depleted region of the BARD1 IDR is labeled and indicated by a black bar.

F Schematic of asymmetric di-NCP substrates architecture.

G, H Quantification of time-course H2A-Ub assays using the indicated combinations of di-NCP substrate and BRCA1/BARD1 heterodimer. In each case, the y-axis reports on the fraction of H2A^{observe} (as shown in Panel F). Lower E3 concentrations were used in these reactions than in those presented in Fig 1 using unmodified mono-nucleosome substrates (15 nM vs. 100 nM), accounting for the slower observed H2A-Ub kinetics for the unmodified di-nucleosome substrate.

Data information: For panels (B, C, D, G, and H), data show the mean; error bars are ±1-s.d. of n = 3 independent technical replicate experiments. One time-point from panel (D) was determined to be an outlier due to a reaction quenching error and excluded from analysis. The excluded value is reported as source data. Source data are available online for this figure.

Effects of H2A-Ub marks on BRCA1/BARD1 H2A-Ub activity

Effects of mono-Ub at H2A positions known to be ubiquitylated by different E3 ligases were assessed using homogeneously mono-ubiquitylated nucleosomes containing ubiquitin preinstalled at H2A positions K15, K119, or K127 via a nonhydrolyzable dichloroacetone cross-linker (Appendix Fig S7B and C) (Morgan *et al*, 2019). Ubiquitin at either H2A C-terminal position (K119 or K127) decreased BRCA1/BARD1-dependent H2A-Ub activity, hinting at exclusivity between BRCA1/BARD1 and RING1/PCGF E3 complexes that both modify in the H2A C-terminal tail region. Consistent with previous observations, Ub preinstalled at H2A K15 increased the H2A-Ub activity of full-length BRCA1/BARD1, and this enhancement requires BARD1 CTDs (Figs 6D and EV5B, Appendix Fig S7D). This contrasts with unmodified nucleosome substrates where BARD1 CTDs are not required for enhanced H2A-Ub activity (Hu *et al*, 2021).

H2A K15-Ub-mediated enhancement of BRCA1/BARD1 H2A-Ub activity

Binding of BARD1 CTDs to nucleosomes that contain both H2A K15-Ub and H4K20me0 (Dai *et al*, 2021; Hu *et al*, 2021) recruits BRCA1/BARD1 to damaged chromatin to facilitate DNA DSB repair via HR (Nakamura *et al*, 2019; Becker *et al*, 2021; Kraiss *et al*, 2021). The BARD1 CTDs use a binding surface that overlaps with the RING domain site, precluding binding of both domains to the same nucleosome face. However, the observation that nucleosomes containing H2A K15-Ub and H4K20me0 are better substrates in the context of BARD1^{FL} implies that RING domains and CTDs can bind simultaneously to opposite faces of a nucleosome (Hu *et al*, 2021). We used BARD1 truncation constructs to determine what features of BARD1 contribute to enhanced activity on H2A K15-Ub nucleosome substrates. As expected, deletion of the CTDs or histone-binding RING mutations of BARD1 do not support activity (Fig 6D). Deletion of the BARD1 DNA-binding IDR (BRCA1^{RING}/BARD1^{Δ140–270}) led to decreased H2A-Ub kinetics compared with the BRCA1^{RING}/BARD1^{FL} complex (Fig 6D). Thus, even with the additional nucleosome-binding contribution provided by the CTDs on H2A K15-Ub nucleosomes, the DNA-binding IDR still plays a role in enhancing ubiquitylation kinetics. Altogether, our findings support a model in which three points of contact between BARD1 and H2A K15-Ub nucleosomes (RING-histone, IDR-DNA, and CTDs-histone/Ub) are required for full BRCA1/BARD1-dependent H2A-Ub activity.

Chemical cross-linking experiments using amino-reactive cross-linkers DSS and BS3 and analyzed by mass spectrometry were carried out to compare complexes formed on unmodified versus H2A K15-Ub-modified nucleosomes (Appendix Fig S8A–C). To focus on the BARD1 subunit, BRCA1^{RING}/BARD1^{FL} was used. There were clear differences in cross-linked products involving BARD1 CTDs, with numerous intermolecular cross-links (judged by unique cross-links and peptide spectral mapping counts) to nucleosomes containing H2A K15-Ub but only sparse cross-links from reactions that included unmodified nucleosomes (Figs 6E and EV5C). The cross-links detected are consistent with high-resolution structures of BARD1 CTDs bound to nucleosomes containing H2A K15-Ub and the lack of these in the unmodified nucleosome reaction is consistent with the interaction being critically dependent on the presence

of Ub at H2A K15 (Appendix Fig S8C). There was also increased cross-linking between BARD1 RING and IDR domains to histones in samples containing H2A K15-Ub nucleosomes (Fig 6E, gray cross-links and Fig EV5C and D), consistent with the reported higher binding affinity of that complex. Thus, binding of the BARD1 CTDs in response to the presence of H2A K15-Ub facilitates BARD1 RING and IDR interactions that lead to the observed increase in H2A K127-Ub activity.

The BARD1 RING domain and CTDs are separated by ~300 intrinsically disordered residues, allowing for as much as 1,000 Å of separation between the two structured domains. It is therefore possible that the CTDs bind to one nucleosome unit, while the RING domains are recruited to a nearby nucleosome unit on chromatin to facilitate H2A-Ub activity. To test this possibility explicitly, asymmetric di-nucleosome substrates (di-NCPs) where one nucleosome unit contained H2A K15-Ub (H2A^{silent}) and an adjacent nucleosome unit contained unmodified H2A with a fluorophore conjugated near its N-terminus to facilitate specific detection in a nucleosome ubiquitylation assay were assembled (Fig 6F, Appendix Fig S9A–C). The nucleosome tethered to a K15-Ub partner nucleosome (denoted as H2A^{observe}) was rapidly ubiquitylated by BRCA1^{RING}/BARD1^{FL} and this level of activity requires the BARD1 CTDs (Figs 6G and EV5E). Unmodified di-NCPs were ubiquitylated with similar kinetics regardless of the presence or absence of the CTDs. Similar activity enhancement dependent on the presence of H2A K15-Ub was observed using full-length BRCA1/BARD1 and asymmetric dinucleosome substrates (Fig EV5F). The presence of equal amounts of unlinked silent H2A K15-Ub nucleosomes and unmodified mononucleosomes (H2A^{observe}) had no effect on H2A-Ub activity (Fig EV5G). The results confirm that BARD1 CTDs bound to an H2A K15-Ub-containing nucleosome enable RING binding to a neighboring nucleosome and that this configuration leads to high ubiquitylation activity. Furthermore, deletion of the BARD1 DNA-binding IDR yields a substantial loss of H2A-Ub activity, indicating that all three binding functionalities are required for full activity (Fig 6H). Altogether, the results support formation of a higher order chromatin complex where BARD1 spans adjacent nucleosome units in which at least one contains H2A K15-Ub. The complex is mediated through binding of the BRCA1/BARD1 RING domains and BARD1 CTDs to neighboring nucleosome units and of the BARD1 IDR to intervening linker DNA.

Discussion

Structural and biochemical studies have revealed that the two RING domains of heterodimeric BRCA1/BARD1 bind to the histone face of a nucleosome and that this interaction is essential for the ability to modify histone H2A at its C-terminal tail (Hu *et al*, 2021; Witus *et al*, 2021a). Other studies revealed that the BARD1 CTDs also binds to the histone face, but this interaction requires Ub-modified H2A, a modification that occurs in response to DNA damage (Becker *et al*, 2021; Hu *et al*, 2021; Kraiss *et al*, 2021). Herein we have identified an additional region of BARD1 that engages with chromatin, namely the BARD1 IDR proximal to the RING (IDR^{prox}). In concert with the RING domains, BARD1 IDR^{prox} is sufficient to support highly enhanced H2A-Ub activity *in vitro*. Multivalent interactions involving the BARD1 IDR^{prox} and the RING domains increase the

apparent binding affinity of the complex from a micromolar to nanomolar binding regime, likely critical in cells where BRCA1/BARD1 is in low abundance. Indeed, our cellular data reveal an important role for this region in chromatin recruitment under both basal and DNA damage conditions and in DNA damage repair. Remarkably, this critical function is carried out by a short stretch of intrinsically disordered BARD1 residues that are highly conserved.

We propose distinct complexes of BRCA1/BARD1 and chromatin substrates that depend on the status of nucleosomal histone PTMs (e.g., unmodified or H2A K15-Ub) (Fig 7A–F). Importantly, while BARD1 CTDs are critical for interactions with nucleosomes that contain H2A K15-Ub, they are dispensable for high-affinity interactions with unmodified nucleosomes (Fig 7C and D). Additional interactions that enhance H2A-Ub activity are mediated through BARD1 IDR^{prox} which engages nucleosomal and extra-nucleosomal linker DNA. Our findings indicate that DNA binding plays an auxiliary role in the ability of BRCA1/BARD1 to ubiquitylate H2A by boosting the affinity of the Ub ligase/nucleosome complex. Supporting this, a BARD1 RING-domain mutant (BARD1 P89A/W91A) that disrupts histone binding is

unable to support H2A-Ub activity with any chromatin substrate tested despite retaining strong nucleosome binding affinity and intrinsic Ub ligase activity. This indicates that high-affinity binding to nucleosomal DNA by BARD1 IDR^{prox} is not sufficient for H2A-Ub activity and that the positioning of the RING domains on the histone surface to orient the RING-E2 ~ Ub complex for site-specific ubiquitin transfer to histone H2A is absolutely required.

BARD1 IDR^{prox} contains two discrete regions with DNA-binding properties, separated by ~30 residues. Each DNA-binding region has a high Lys/Arg content while the intervening region contains more negatively charged residues (Fig EV2C). The more C-terminal residues of BARD1 IDR^{prox} (190–216) appear to be the dominant site for dsDNA engagement while the portion of BARD1 IDR^{prox} (145–165) directly adjacent to the RING domain also engages dsDNA but shows a pronounced preference for specialized DNA structures such as bubble-DNA that have features found in intermediates in HR (Zhao *et al*, 2017) and possibly in R-loop structures formed during transcription (Santos-Pereira & Aguilera, 2015). The two regions display different secondary structure propensities, and we note a

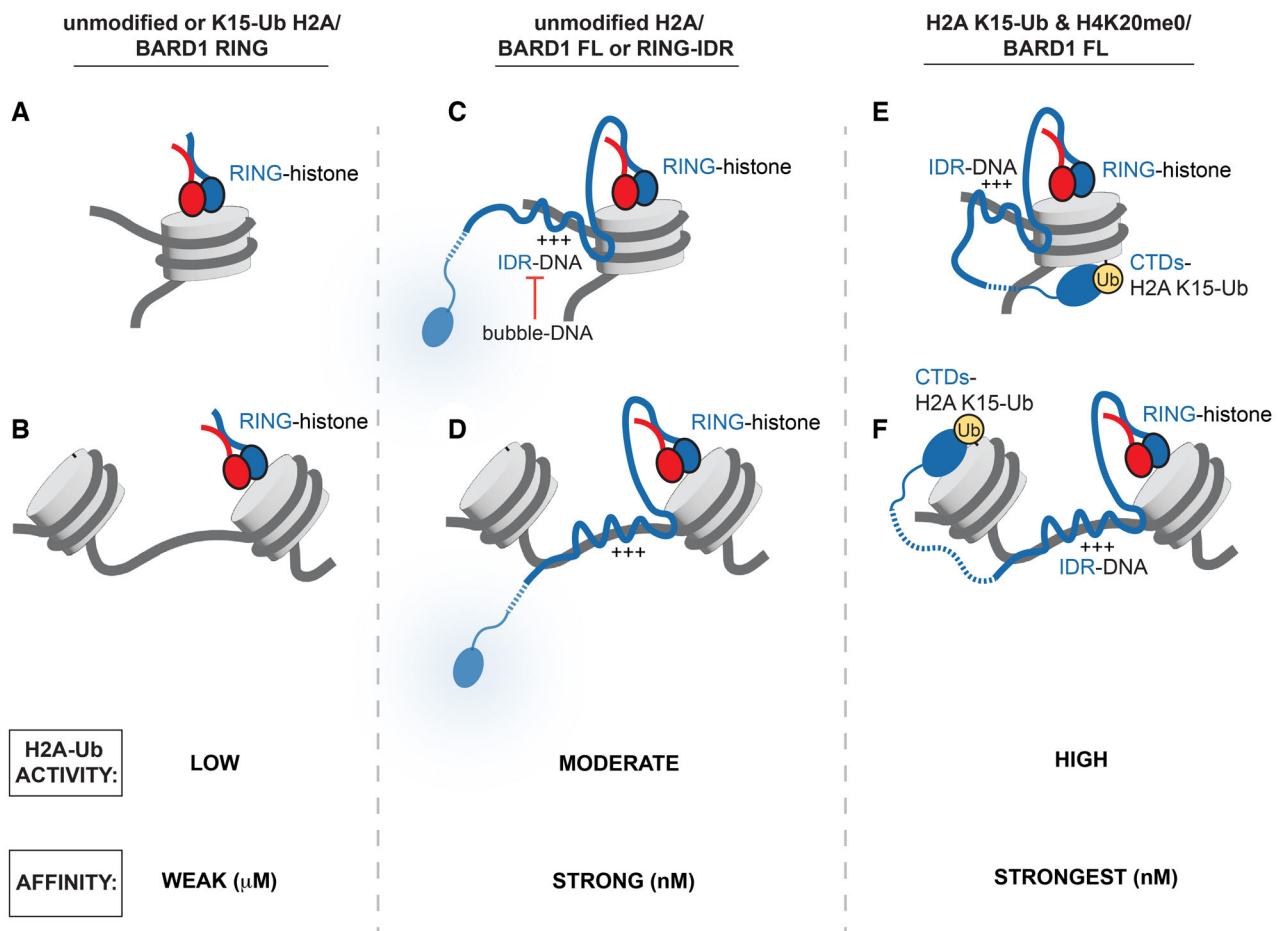


Figure 7. Models of BRCA1/BARD1/chromatin complexes supported by this study.

A, B Model of the BRCA1/BARD1 minimal RING heterodimer binding to an unmodified mono-nucleosome or higher order chromatin substrate.
 C, D Model of BRCA1/BARD1 (BARD1 full-length or RING-IDR) binding with an unmodified mono-nucleosome or higher order chromatin substrate.
 E, F Model of BRCA1/BARD1^{FL} binding to ubiquitylated chromatin substrates as a “wrapped complex” (panel E) or as a complex that spans nucleosome units (panel F).
 The relative H2A-Ub activity and affinity of the complexes are indicated below each set of panels.

conserved hydrophobic trio (145-MWF) within the RING-adjacent site that is highly affected by bubble-DNA. Structural information regarding IDR-DNA interactions is sparse, but our findings hint at distinct modes of binding by IDRs rather than merely electrostatic, non-specific associations. To that point, BARD1 IDR^{prox} appears to possess small regions with specialized binding modes that are linked to BRCA1/BARD1 function.

Preferential binding to bubble-DNA serves to inhibit H2A-Ub activity in our assays in which the specialized DNA species was present *trans*. This suggests the intriguing possibility that proximity or high local concentrations of such species might modulate the modification of H2A by BRCA1/BARD1 in cells. Furthermore, binding of BARD1 IDR^{prox} to nucleosomal DNA or to specialized nucleic acid structures could serve to control its spatial and temporal involvement in HR and other processes where such specialized DNA structures may be present (e.g., stalled replication fork protection, and R-loop resolution) (Schlachter *et al*, 2012; Hatchi *et al*, 2015). Additionally, BRCA1/BARD1 is present in higher order protein assemblies that are known to bind to chromatin via distinct nucleosome interfaces that may be formed by other proteins in the complex (Bochar *et al*, 2000; Huen *et al*, 2010; Savage & Harkin, 2015; Belotserkovskaya *et al*, 2020). Understanding the combined binding contributions of BRCA1/BARD1 and other proteins in such complexes to nucleosome association and H2A-Ub activity is an important future goal.

Data presented here provide direct experimental evidence in support of an extended BRCA1/BARD1/chromatin complex that spans nucleosomal units. Such a complex is enabled by the presence of H2A K15-Ub, an early mark of DNA damage, which engages the BARD1 CTDs while the enzymatic RING domains occupy an adjacent/nearby nucleosome unit (Fig 7E and F). The 300-residue BARD1 IDR allows extensive separation between the enzymatic RING domains and BARD1 CTDs while itself engaging in high-affinity interactions with nucleosomal/linker DNA. Such a configuration may allow the RING domains to reach nucleosome units even further away than an adjacent unit while anchored to chromatin via the BARD1 CTDs. This situation could lead to BRCA1/BARD1-dependent H2A-Ub of multiple nucleosomes in the vicinity of a H2A K15-Ub anchor nucleosome. Additionally, the ability to reach across nucleosome units in chromatin provides a platform to scaffold higher order complexes across long molecular distances.

As H2A K15-Ub is specifically a mark of DNA damage, this model will not be in play for other BRCA1/BARD1-dependent processes on chromatin such as its transcriptional repression and activation activities. Results presented here show that the DNA-binding BARD1 IDR^{prox} is required for enhanced H2A-Ub activity on unmodified nucleosomes. An important question going forward is what other histone PTMs influence the chromatin binding and H2A-Ub activity of BRCA1/BARD1. We previously reported that methylation at H3 K79, a mark associated with actively transcribed chromatin, inhibits BRCA1/BARD1-mediated H2A-Ub activity (Witus *et al*, 2021a). This may be attributable to the location of H3 K79 near the BARD1-histone interface. A comprehensive understanding of histone PTMs that influence BRCA1/BARD1 nucleosome binding, higher order chromatin complex formation, and H2A-Ub activity will provide valuable insight into its functions and regulation in different biological processes.

Mostly missing from our discussion is the huge BRCA1 subunit. Its only established direct point-of-contact to chromatin is via its N-terminal RING domain, although at least one section of its

enormous IDR has DNA binding activity *in vitro* (Mark *et al*, 2005). BRCA1/BARD1 serves as a large protein interaction hub that forms numerous distinct complexes, many of which involve BRCA1 as the binding partner. In our *in vitro* investigation, the entirety of BRCA1 apart from its enzymatic RING domain, was dispensable for H2A-Ub activity. That said, we note that full-length BRCA1/BARD1 displayed lower H2A-Ub activity than complexes containing truncated BRCA1 (Δ 11q or RING) and offer two hypotheses for the observation. First, BRCA1^{FL} but neither truncation contains a DNA-binding region that supports lower H2A-Ub activity than BARD1 IDR^{prox}. This lower activity may be due to a longer tethering distance between the BRCA1 DNA-binding regions and the enzymatic RING domains that bind to the histone surface, or other intrinsic differences in nucleosomal DNA binding capabilities compared to BARD1 IDR^{prox}. Thus, the presence of strong DNA-binding regions in both BRCA1 and BARD1 in the full-length complex could set up a competition between these regions for binding to nucleosomal DNA, leading to lower apparent H2A-Ub activity stemming from the BRCA1 DNA-bound population. Alternatively, or in addition, possible inhibitory interactions between BRCA1 and BARD1 subunits might have been alleviated upon BRCA1 truncation. Although such effects could be artifactual, we suggest that the status of the BRCA1 subunit in terms of its binding partners could provide an additional layer of modulation of BRCA1/BARD1 H2A-Ub activity. Occupancy of regions of BRCA1 and BARD1 by unique binding partners may occlude certain nucleosome-binding regions, resulting in inhibition or enhancement of chromatin binding and H2A-Ub activity. Further investigation into chromatin complexes containing full-length BRCA1/BARD1 and the many protein assemblies and binding partners that are required to execute its cellular functions is warranted.

In conclusion, our results establish an extensive multivalent network of interactions that facilitate BRCA1/BARD1 chromatin association and H2A-Ub activity. These interactions are likely critical for many functions of BRCA1/BARD1 in the nucleus that are not limited to its H2A-Ub activity and may be disrupted by mutations that cause cancer.

Materials and Methods

Protein, nucleosome, and experimental reagent production

Ubiquitylation machinery

Human E1 (UBA1), E2 (UBE2D3), and ubiquitin (wild-type and Q2C mutant) were expressed and purified as previously described (Lazar *et al*, 1997; Brzovic *et al*, 2003; Christensen *et al*, 2007). For a full list of BRCA1/BARD1 truncation constructs, their residue bounds, purification/epitope tags, and expression system, see Appendix Table S1.

BRCA1/BARD1 from *E. coli*

For purification of truncated BRCA1/BARD1 heterodimers from *E. coli* expression (BRCA1^{RING}/BARD1^{RING}, BRCA1^{RING}/BARD1¹⁹³, and BRCA1^{RING}/BARD1²¹⁶), plasmids containing 6xHis-tagged BRCA1 (pCOT7n) and untagged BARD1 (pET28n) were co-transformed into *E. coli* BL21 (DE3) cells, grown in LB media at 37°C to OD_{600nm} of 0.6–0.8, supplemented with 100 μ M ZnCl₂ and induced with 0.2 mM IPTG for ~16 h at 16°C. The cell pellets were resuspended in 30 ml

of Ni²⁺ start buffer (25 mM Tris-HCl pH 7.5, 500 mM NaCl, 10 mM imidazole) supplemented with DNase, RNase, EDTA-free protease inhibitors (Roche) and 1 mM PMSF, lysed by French press, centrifuged, and the supernatant was applied to a 5 ml HisTrap FF crude column (Cytiva). After extensive washing with Ni²⁺ start buffer containing 10 mM imidazole and 30 mM imidazole, protein was eluted using the same buffer supplemented with 500 mM imidazole. The BRCA1^{RING}/BARD1^{RING} and BRCA1^{RING}/BARD1¹⁹³ constructs were concentrated and further purified using a 120 ml Superdex 75 column on an AKTA FPLC system in SEC buffer (25 mM HEPES-NaOH pH 7.5, 150 mM NaCl, 1 mM DTT; GE Healthcare). For the BRCA1^{RING}/BARD1²¹⁶, HisTrap elutions were dialyzed into ion-exchange buffer (25 mM Tris-HCl pH 7.5, 250 mM NaCl, 1 mM DTT) and applied to a 5 ml HiTrap SP HP column (Cytiva) and eluted over a 12 column-volume (CV) gradient (0.25–1 M NaCl). Peak fractions were concentrated, aliquoted, and flash frozen.

For Bpa cross-linking experiments, 6xHis-BRCA1^{1–104}-(GS)₆-BARD1^{26–221} was subcloned using Gibson assembly into a pET28n vector. Constructs for Bpa incorporation were generated via site-directed mutagenesis to install amber stop codons in place of BARD1 L120, W146, Y180, A195, and W218. Bpa-mutant Pet28n-6xHis-BRCA1^{1–104}-(GS)₆-BARD1^{26–221} plasmids were co-transformed with a pEVOL-pBpF plasmid encoding an Bpa aminoacyl tRNA synthetase (gift from P. Schultz, Addgene #31190) in *E. coli* BL21 (DE3) cells (Chin *et al.*, 2002). At OD_{600nm} = 0.4–0.5, cells were shifted from 37 to 16°C and supplemented with 1 mM Bpa (dissolved in 1 M NaOH; Bachem) and 100 μM ZnCl₂. After 30 min, protein expression was induced by addition of 0.02% L-arabinose and 0.2 mM IPTG for ~16 h at 16°C. Proteins were purified as described for the BRCA1^{RING}/BARD1²¹⁶ construct. Truncations that did not incorporate Bpa were separated via the SP column.

BRCA1/BARD1 from insect cells

For insect cell expression, truncation and deletion constructs were derived from full-length BRCA1 (pFastBac-FLAG-BRCA1^{1–1863}; gift from W. Zhao, UT Health Sciences Center at San Antonio) and insect cell codon-optimized full-length BARD1 (pFastBac-Twin-StrepTagII-BARD1^{1–777}; gift from A. Deans, Addgene plasmid #137166) (Tan *et al.*, 2020) using Gibson assembly cloning (NEB). Baculovirus was generated using the Bac-to-Bac system in suspension culture Sf9 cells according to the manufacturers protocols (Invitrogen). For general Sf9 growth and virus amplification, SF900-II media (ThermoFisher) was supplemented with 5% FBS (HyClone) and 1× antibiotic-antimycotic (Gibco). For protein expression, 15 ml of BRCA1- and 15 ml of BARD1-containing P3 baculoviruses were added to 650 ml of Sf9 cells at ~1.5 × 10⁶ cells/ml in SF900-II media supplemented with 1% FBS and 1× antibiotic-antimycotic. Protein expression was carried out for 48–72 h at 27°C, shaking at 110 RPM. Following expression, cells were spun down at 300 × g for 10 min. The pellet was resuspended in 30 ml of Strep-start buffer (50 mM Tris-HCl pH 8, 10% glycerol, 150 mM NaCl, 1 mM DTT) supplemented with EDTA-free protease inhibitors and 1 mM PMSF and flash-frozen. Following freeze-thawing in a 37°C water bath, additional EDTA-free protease inhibitors and PMSF were added in addition to 2 μl of benzamide (Sigma Aldrich). All subsequent steps were performed on ice or in a cold room over a short timeframe to prevent proteolysis (< 3 h total). Lysis was performed by sonication using a Branson Sonifier 250 (VWR Scientific) by applying 2 rounds of 15 pulses at 70% duty on

power level 8, ensuring that the cell mixture stayed cold. PMSF was added throughout the lysis protocol. The lysed cells were centrifuged at 41,000 × g for 15 min, filtered through a 0.45 μm low protein-binding PVDF filter (Millipore), and applied to a 1 ml StrepTrap HP column pre-equilibrated in Strep-start buffer (Cytiva). The column was washed with 8 ml Strep-start buffer supplemented with protease inhibitors, 8 ml wash buffer (25 mM Tris-HCl pH 7.5, 300 mM NaCl, 0.01% Igepal-CA630, 1 mM DTT, 5 mM MgCl₂, 2 mM ATP, 10% glycerol, EDTA-free protease inhibitors), and an additional 5 ml of Strep-start buffer. The column was eluted using 6 ml of Strep-start buffer supplemented with 3 mM d-Desthiobiotin (Sigma). The elution was diluted with 20 ml of ion-exchange buffer (25 mM HEPES-NaOH pH 7.5, 10% glycerol, 1 mM DTT) and applied to a 1 ml SP HP column pre-equilibrated in ion-exchange buffer containing 75 mM NaCl. The SP column was eluted over 12-CV (75–500 mM NaCl). Peak fractions were combined and concentrated using a 30K MWCO concentrator (Amicon) and flash-frozen in small aliquots. Concentrations were estimated by measuring absorbance at 280 nm using molar extinction coefficients obtained from ProtParam (ExPasy). Concentration estimates were verified by SDS-PAGE and Coomassie staining, and slight adjustments in concentration were applied to best equalize the amounts of E3 in activity and binding assays.

BARD1 intrinsically disordered region

BARD1 124–270, 141–216, 269–424, and 124–424 were subcloned from pFastBac-6xHis-BARD1^{1–777} (gift from W. Zhao, UTHSCA) into a modified pET28 vector containing an N-terminal 6xHis-SUMO tag using Gibson assembly cloning. Plasmids were transformed into BL21 (DE3) *E. coli*, grown at 37°C in M9 media supplemented with appropriate combination of isotopes (¹⁵N-NH₄Cl, ¹³C-glucose; Cambridge Isotopes) to an OD_{600nm} of 0.6–0.8, and induced with 0.2 mM IPTG for ~16 h at 16°C. HisTrap Ni²⁺ purification was performed as described above for BRCA1/BARD1 constructs expressed in *E. coli*. Elutions were dialyzed into ion exchange buffer (25 mM Tris pH 8.0, 200 mM NaCl, 0.5 mM EDTA, 1 mM DTT) in the presence of GST-SENPI (produced in-house) to cleave the SUMO tag, leaving a non-native serine residue preceding the N-terminus except in the case of 269–424. The cleaved product was applied to a HiTrap Q column preceding a HiTrap SP column in-tandem to capture the non-specifically bound DNA (Cytiva). After application, the Q column was removed, and the SP column was eluted using a 12-CV gradient (0.2–1 M NaCl). The peak fractions were combined, concentrated, and further purified using a Superdex 75 column equilibrated in NMR buffer (25 mM MOPS-NaOH pH 7.0, 100 mM NaCl, 1 mM EDTA, 0.5 mM TCEP (tris(2-carboxyethyl)phosphine)).

Histone purification

Wild-type and mutant human histones were transformed in *E. coli* BL21 (DE3) pLysS cells, grown at 37°C to an OD_{600nm} of 0.5–0.6, and induced with 0.5 mM IPTG for 2 h (H4) or 3 h (H2A-2A, H2B-1 K, H3.2) at 37°C. Histone octamers used for fluorescence labeling were purified using the one-pot refolding protocol as described previously using 6xHis-TEV-H2A (Lee *et al.*, 2015; Witus *et al.*, 2021a). For nucleosome ubiquitylation assays, a glycine within the TEV cleavage scar was mutated to a cysteine for fluorophore conjugation (H2A G-1C) via site-directed mutagenesis. For fluorescence-based binding assays, a cysteine was introduced at H2B D51 via site-directed mutagenesis.

For reconstituting chemically modified H2A-Ub nucleosomes, histones were purified individually essentially as described (Luger *et al.*, 1999). Briefly, inclusion bodies from 6 to 8 l of histone expression in LB media were lysed in buffer T (50 mM Tris-HCl pH 7.4, 1 mM EDTA, 100 mM NaCl), washed by sonication twice in buffer TW (50 mM Tris-HCl pH 7.4, 1 mM EDTA, 100 mM NaCl, 1% v/v Triton-X100), and then twice again in buffer T. Inclusion bodies were softened by stirring with a small volume of DMSO (2–3 ml), and extracted with 60 ml of extraction buffer (25 mM Tris-HCl pH 7.5, 7 M guanidinium-HCl, 0.5 mM EDTA, 10 mM DTT). After centrifugation, the supernatant was dialyzed overnight into ion-exchange buffer (25 mM Tris-HCl pH 7.5, 7 M deionized urea, 100 mM NaCl, 0.5 mM EDTA, 10 mM DTT) and applied to 2 × 5 ml HiTrap Q columns preceding 2 × 5 ml HiTrap SP columns in-tandem to capture the non-specifically bound DNA (Cytiva). After sample application, the Q columns were removed, and the SP columns were eluted using a 12-CV salt gradient (0.1–1 M NaCl for H2A and H2B, 0.2–1 M NaCl for H3 and H4). The peak fractions were assessed by Coomassie stained SDS-PAGE gel and Abs₂₆₀/Abs₂₈₀ value, and the purest fractions were extensively dialyzed into water, aliquoted, flash frozen, and lyophilized. Lyophilized histones were reconstituted into H2A/H2B dimers, H3/H4 tetramers, and octamers as previously described (Dyer *et al.*, 2003), and purified via SEC using Superdex 75 (H2A/H2B) or Superdex 200 (H3/H4 and octamers) columns in SEC buffer (25 mM Tris-HCl pH 7.5, 2 M NaCl, 1 mM DTT).

Fluorophore conjugation to histones and ubiquitin

For fluorophore conjugation, AlexaFluor 680 C₂ maleimide (ThermoFisher), IRDye 680LT maleimide (Li-Cor), and Oregon green 488 maleimide (AAT Bioquest) were reconstituted in DMSO to 10 mM. Fluorophore maleimides were mixed with octamers containing single cysteine mutants H2A G-1C for H2A-Ub activity assays (with Alexa Fluor 680 C₂ maleimide or IRDye 680LT maleimide) or H2B D51C for binding assays (with Oregon green 488 maleimide). Conjugation reactions were performed using 20 μM octamer and 100 μM fluorophore overnight at 4°C in conjugation buffer (25 mM Tris-HCl pH 7.5, 2 M NaCl, 1 mM EDTA, 0.5 mM TCEP), and stopped by addition of 10 mM DTT and flash frozen. Excess fluorophore was removed after nucleosome reconstitution by SEC using a Superdex 200 increase 10/300 GL column or extensive buffer exchange in a 30 K MWCO concentrator (Amicon). Typical labeling efficiency was ~70%. For labeling of Ub Q2C, 100 μM Alexa Fluor 680 C₂ maleimide was mixed with ~1 mM of Ub Q2C in buffer (25 mM Tris-HCl pH 7.5, 1 mM EDTA, 0.5 mM TCEP) at 4°C overnight. The reaction was quenched with 10 mM DTT, and buffer exchanged into reducing buffer (25 mM Tris-HCl pH 7.5, 1 mM EDTA, 10 mM DTT) in a concentrator to remove unconjugated dye, and stored at –80°C. The fluorophore labeling efficiency of Ub was calculated to be ~5%.

Ubiquitin G76C and dichloroacetone cross-linking of H2A-Ub

H2A K15C, K119C, and K127C were generated by site-directed mutagenesis and purified as described above for individual histones. His-TEV-ubiquitin G76C was a gift from C. Wolberger (Addgene plasmid #75299) and purified as previously described (Morgan *et al.*, 2016, 2019). Dichloroacetone cross-linking of Ub G76C to H2A single cysteine mutants was performed as previously described in detail (Morgan *et al.*, 2019), with the exception that the final product containing

Ub, Ub-Ub dimers, and H2A-Ub was not purified by RP-HPLC to remove unconjugated Ub. Instead, it was lyophilized, and mixed with a slight excess of H2B in unfolding buffer (25 mM Tris-HCl pH 7.5, 7 M guanidinium-HCl, 0.5 mM EDTA, 1 mM DTT), refolded into H2A/H2B dimers in refolding buffer (25 mM Tris-HCl pH 7.5, 2 M NaCl, 1 mM DTT), and purified by SEC using a 24 ml Superdex 75 column (GE Healthcare) to separate the H2A-Ub from Ub species.

“601” and MMTV DNA

For large-scale purification of 147-bp “601” (gift from K. Luger, CU Boulder), 185-bp “601” (gift from S. Tan, Penn State Univ.), MMTV (gift from G. Debelouchina, UC San Diego), and NLE-trimer “601” (for tri-NCP; gift from K. Luger) DNA, repeat plasmids from 8 to 12 l of DH5a cells in LB media were subjected to alkaline lysis, phenol-chloroform extraction, PEG precipitation, EcoRV digestion (NEB), and ion exchange of the excised fragment by HiTrap DEAE (147-bp “601,” 185-bp “601,” and MMTV; Cytiva) or mono-Q (NLE-trimer “601”; GE Healthcare) according to established protocols (Dyer *et al.*, 2003).

For UV-induced Bpa cross-linking and EMSA experiments, fluorophore labeled “601” DNA was generated using large-scale PCR with Phusion polymerase (produced in-house) from a pGEM-3z/601 plasmid containing one copy of “601” DNA (gift from J. Widom, Addgene plasmid #26656) (Lowary & Widom, 1998) with 5'-IRDye700 labeled forward primers (IDT). Following PCR, the reactions were purified using a 1 ml mono-Q column equilibrated in ion-exchange buffer (25 mM Tris-HCl pH 8.0, 200 mM NaCl, 1 mM EDTA) over a 10-CV gradient (0.2–1 M NaCl). Peak fractions containing purified 147- and 185-bp DNA fragments were dialyzed into storage buffer (10 mM Tris-HCl pH 8.0, 1 mM EDTA), concentrated, and stored at –20°C. The primer sequences were as follows: 147-fwd: ctggagaatcccgggtgccgagg; 147-rev: acaggatgtatatactgacacg; 185-fwd: atccctatacgcggcgccctggagaatcccgggtgccgagg; 185-rev: atcgctgtcaatacagcacaggatgtatatactgacacg.

For generation of DNA fragments with DraIII sticky ends for dinucleosome assembly, large-scale PCR was performed as described for the fluorophore-labeled DNA fragments above. Primer sequences containing DraIII cut-sites were based off those used by Poepsel *et al.* (2018) to make dinucleosomes with 35-bp of linker DNA. Fragments used to reconstitute nucleosomes containing fluorophore-labeled H2A nucleosomes (H2A^{observe}) were generated using the “147-fwd” primer (sequence above) and the di-NCP reverse primer sequence (taggtatcgtatCACGGGGTGagatcgctacag-gatgtatatactgacacg). The fragment for the H2A^{silent} nucleosomes was generated using the “147-rev” and the di-NCP-forward primer sequence (ctgactattgaCACCCCGTGatgctcgtactgtcactatggagaatcccgtgccgag). The DraIII sites in the primers are underlined and uppercase. Following PCR purification by 1 ml mono-Q, DNA fragments were dialyzed into TE/0.1 buffer (10 mM Tris-HCl, 0.1 mM EDTA) and digested with DraIII-HF in 1 × CutSmart buffer for ~20 h at 37°C (NEB). Fragments with DraIII sticky ends were repurified by 1 ml mono-Q ion-exchange, dialyzed into storage buffer (10 mM Tris-HCl, 1 mM EDTA), concentrated, and stored at –20°C.

Nucleosome reconstitution

Mono-nucleosome core particles were reconstituted by the standard salt-dialysis method by mixing histone octamers (or H3/H4 tetramers and H2A/H2B dimers) with “601” DNA in high salt buffer (25

mM Tris-HCl pH 7.5, 2 M NaCl, 0.1 mM EDTA, 1 mM DTT) in a slide-a-lyzer mini dialysis unit (0.1 ml, ThermoFisher) (Dyer et al, 2003). Low-salt buffer (25 mM Tris-HCl pH 7.5, 0.1 mM EDTA, 1 mM DTT) was pumped in over ~24 h in a cold room with stirring. A final dialysis was performed into NCP storage buffer (25 mM HEPES-NaOH, 10 mM NaCl, 0.1 mM EDTA, 1 mM DTT). Fluorophore-labeled nucleosomes were further purified by SEC using a 24 ml Superdex 200 increase 10/300 column equilibrated in NCP storage buffer or by extensive buffer exchange in a concentrator to remove excess fluorophore. For tri-NCPs, salt dialysis was performed as described for mono-NCPs using ~1.4× octamer to “601” sites in the presence of 0.2 equivalents of MMTV competitor DNA. Following dialysis into TEK10 (10 mM Tris-HCl pH 7.5, 0.1 mM EDTA, 10 mM KCl), trimers were precipitated by adding 4 mM MgCl₂, incubating on ice for 10 min and pelleted by centrifugation at 17,000×g at 4°C. The supernatant was discarded, and the pellet was gently resuspended in TEK10, and dialyzed overnight into NCP storage buffer. Tri-NCP assembly was verified by EcoRI digestion of sites located between nucleosome units.

For di-NCP assembly, mono-NCPs with DraIII sticky ends were assembled as described above. The strategy to make asymmetric di-NCPs was based on previously described methods (Poepsel et al, 2018; Dao et al, 2020). 100 nM of each NCP was mixed in T4 ligase buffer (50 mM Tris-HCl pH 7.5, 10 mM MgCl₂, 1 mM ATP, and 10 mM DTT) on ice. T4 ligase (NEB) was added to a final concentration of 20 U/μl, the reaction was incubated for 30 min at 16°C and dialyzed into TEK10 for 4 h at 4°C. Following dialysis, MgCl₂ was added to a final concentration of 18 mM, incubated at room temperature for 15 min, and pelleted at 17,000×g at 4°C. The pellet containing di-NCPs was resuspended in 50 μl of TEK10 and dialyzed overnight into NCP storage buffer. All chromatin substrates were analyzed for quality on 5% polyacrylamide 0.5× TBE gels monitoring fluorescence and/or DNA staining, ensuring minimal free DNA or contaminating species. Chromatin substrates were stored on ice for no longer than 1 month.

Design and assembly of DNA competitor fragments

Single-stranded, double-stranded, bubble, frayed, and single-stranded overhang DNA fragments were assembled by annealing ssDNA oligos (IDT) in IDT duplex buffer (30 mM HEPES-NaOH pH 7.5, 100 mM potassium acetate). Oligo mixtures were heated to 95°C and slowly cooled to 25°C stepwise over 1 h in a thermocycler. For NMR experiments, dsDNA and bubble-DNA were buffer exchanged into NMR buffer in a spin concentrator (Amicon). The sequences of oligos used are as follows. For ssDNA, dsDNA, bubbleDNA, and ssOverhang a common “bottom” oligo was used (ggtagcacaattgcgctgtaccacaggcgtgtagg). The oligos annealed to the “bottom” oligo were as follows: (dsDNA-top: cctacgacgacctgggtaccagcgaattgtgtacc; bubbleDNA-top: cctacgacgacctgtcttcccgaattgtgtacc; ssOverhang-top: ccgcaattgtgtac). For the frayed DNA, the annealed oligos were as follows: (frayedDNA-top: ggtacacaattgcgccagcgtgtaggctgtacc; frayedDNA-bottom: ctcttcccctacgacctggcgaattgtgtacc).

Nucleosome ubiquitylation assays

Time-course H2A-Ub assays

The general setup for time-course H2A-Ub assays was a reaction mixture containing 0.2 μM E1 (UBA1), 1 μM E2 (UBE2D3), 30 μM

ubiquitin, 0.5 μM NCP substrate, and 12.5–100 nM E3 (depending on the assay), assembled in 30 μl of reaction buffer (25 mM HEPES-NaOH pH 7.5, 150 mM NaCl). For assays containing di-NCPs, 10 nM of fluorophore-labeled di-NCP substrate was mixed with 0.5 μM unlabeled NCP¹⁴⁷ substrate in the same reaction tube to facilitate quantifiable reaction kinetics. Critically, the salt concentration of each reaction within an assay was rigorously controlled, as H2A-Ub kinetics are extremely sensitive to differences in buffer ionic strength. We note that small changes to buffer ionic strength may occur between individual assays due to the use of different batches of reagents, causing slight differences in activity profiles of the same E3 ligase construct. For this reason, we do not attempt to make quantitative or qualitative comparisons between individual assays. 5 μl of each reaction was mixed 1:1 with 2× SDS-PAGE load dye as a zero time-point. The mixtures were brought to 37°C in a heat block, and 1 μl of 100 mM MgCl₂/ATP was added (4 mM final concentration) to initiate the reaction, and the indicated time-points were obtained by diluting 5 μl the reaction 1:1 with 2× SDS-PAGE load dye. For experiments with tri-NCPs, the concentration of nucleosome units in the reaction was normalized to NCP¹⁴⁷ and NCP¹⁸⁵ (0.5 μM NCP unit or 0.17 μM tri-NCP), and reactions were initiated with 2 mM ATP and 1 mM MgCl₂.

Gel samples were run on 15% SDS-PAGE gels and visualized by in-gel fluorescence monitoring a fluorophore conjugated to the N-terminus of H2A. Alternatively, some assays were visualized by Western blot for H2A (EMD Millipore, 07-146) or a VSVG epitope tag on the N-terminal tag of H2A (Sigma, V4888) and a fluorescently labeled secondary antibody (Cell Signaling, 5151S). Gels and blots were imaged on a Li-Cor Odyssey imager (Li-Cor). Band quantification was performed using Image Studio software (Li-Cor) by drawing a box encompassing the unmodified H2A band to measure its intensity, performing background subtraction, and normalizing to the zero time-point of a given reaction.

Inhibition of H2A-Ub by competitor DNA

A reaction mixture containing 0.2 μM E1 (UBA1), 3 μM E2 (UBE2D3), 30 μM ubiquitin, 0.5 μM NCP substrate, and 50 nM E3 (or 750 nM for BRCA1^{RING}/BARD1^{RING}) was assembled in 9 μl of reaction buffer (25 mM HEPES-NaOH pH 7.5, 100 mM NaCl) in PCR strips. To that, 1 μl of DNA competitor at 10× concentration was added. Reactions were brought to 37°C in a thermocycler, started by addition of 5 μl of 10 mM ATP/MgCl₂ in reaction buffer, and allowed to proceed for 12–20 min depending on the E3. Reactions were stopped by addition of 10 μl of 4× fluorescence sample load dye (Li-Cor), resolved on a 15% SDS-PAGE gel, and visualized using a Li-Cor Odyssey imager. Quantification was performed as described above, monitoring the intensity of unmodified H2A, and normalizing each reaction to a -ATP reaction.

Auto-ubiquitylation assay

Reactions were assembled with 0.2 μM E1 (UBA1), 1 μM E2 (UBE2D3), 10 μM ubiquitin (Q2C-Alexa Fluor 680), and 0.2 μM of the indicated E3 in buffer (25 mM HEPES-NaOH pH 7.5, 50 mM NaCl) and were initiated by addition of 5 mM ATP/MgCl₂. After 60 min at 37°C, reactions were quenched by mixing 1:1 with 4× fluorescence sample load dye (Li-Cor), resolved on a 4–20% SDS-PAGE gel (BioRad), and visualized using a Li-Cor Odyssey imager.

Nucleosome binding assays

Electrophoretic mobility shift assay

For EMSA experiments, 5 μ l of 10 nM of substrate (NCPs with either H2A G-1C labeled with Alexa Fluor 680 or DNA/NCPs labeled with IRDye700) were mixed with 5 μ l of indicated RING/RING heterodimer or BARD1 IDR constructs (2 \times concentrated) in EMSA buffer (15 mM Tris-HCl pH 7.5, 90 mM NaCl, 1 mM DTT, 0.1 mg/ml BSA, 0.05% triton X-100) in PCR strips. Binding was allowed to proceed for 10 min at room temperature, followed by 5 min on ice. 5 μ l of 25% sucrose was added to each tube, and 15 μ l of sample was loaded onto 5% polyacrylamide native gels (0.5 \times TBE) in prechilled 0.5 \times TBE buffer. Gels were run at 4°C for 90–120 min at 110 V and visualized using a Li-Cor Odyssey scanner (Li-Cor).

Fluorescence-quenching binding experiments

Assay set up was performed essentially as previously described (Hu *et al.*, 2021). Ten microliters of about 10 nM NCPs with Oregon green 488 conjugated to H2B D51C in low-salt fluorescence buffer (25 mM Tris-HCl pH 7.5, 10 mM NaCl, 0.01% CHAPS, 0.01% NP40, 0.1 mg/ml BSA, and 1 mM DTT) were mixed with 10 μ l of the indicated BRCA1/BARD1 construct at 2 \times concentration in high-salt fluorescence buffer containing either 90 mM, 190 mM, or 290 mM NaCl, depending on the assay, in a 384-well low volume black round bottom polystyrene non-binding surface microplate (Corning). Plates were briefly mixed, incubated at 22°C for 10–15 min, and scanned using a BioTek Synergy Neo2 plate reader equipped with a fluorescence filter (excitation: 485/20 nm, emission: 528/20 nm). The gain was set to 100 for all experiments. Two to three technical replicates for each independent replicate experiment (fresh NCP and BRCA1/BARD1 dilutions) were performed, and the readings from two scans were averaged. BRCA1/BARD1/nucleosome-binding interactions were quantitatively analyzed by fluorescence quenching assuming the following systems of equations:

$$\theta = \frac{K_D + [NCP] + [BCBD] - \sqrt{(K_D + [NCP] + [BCBD])^2 - 4 \times [NCP] \times [BCBD]}}{2 \times [NCP]}$$

$$F = [NCP] \times F_{NCP} \times (1 - q_{BCBD} \times \theta) + N(0, error)$$

where θ is the fraction of nucleosome bound by BRCA1/BARD1 (BCBD), F_{NCP} is the fluorescence per nucleosome, q_{BCBD} is the fraction of fluorescence quenching per BRCA1/BARD1 binding, and fluorescence measurements are gaussian distributed with mean 0. Maximum likelihood parameter estimates were determined using custom Python scripts with optimization by a differential evolution algorithm implemented in Scipy (Virtanen *et al.*, 2020). K_D and q_{BCBD} were separately estimated for each BRCA1/BARD1 construct, and NCP concentration was treated as a random effect per individual dilutions from higher concentration stock solutions, with the total number of model parameters being equal to number of NCP dilutions + (2 \times number of BCBD constructs) + 2. The 95% confidence limits were estimated by computing the profile likelihood with an applied Bonferroni correction.

UV-induced Bpa cross-linking

Nucleosome core particles and DNA for UV-induced cross-linking assays were reconstituted using a 185-bp “601” sequence labeled

with an IRDye700 fluorophore (described above). About 50 nM NCPs or DNA were incubated with 500 nM of the BRCA1^{1–104}-(GS)₆-BARD1^{26–221} fusion (wild-type or with different Bpa-incorporated sites L120Bpa, W146Bpa, Y180Bpa, A195Bpa, W218Bpa) for 15 min at 4°C in 30 μ l UV cross-linking buffer (20 mM HEPES-NaOH pH 7.5, 100 mM NaCl) in a 96-well clear round bottom polystyrene nontreated microplate (Corning). Following incubation, 5 μ l was added to 5 μ l 2 \times SDS-PAGE gel-loading dye for the -UV sample. Samples were then subjected to UV irradiation (365 nm) using a Blak-Ray B-100AP/R High-intensity UV Lamp (UVP) from 20 cm for 30 min at 4°C. Following irradiation, 5 μ l was added to 5 μ l of 2 \times SDS-PAGE gel-loading dye. Samples were heated at 60°C for 5 min and separated on 10% SDS-PAGE gels. Gels were visualized using a Li-Cor Odyssey scanner (Li-Cor). Band quantification was performed using Image Studio software (Li-Cor) by drawing a box measuring the total band intensity for each cross-linked product, subtracting the background signal, and normalizing to the cross-linked band of the L120Bpa fusion mutant. For the Bpa UV cross-linking DNA competition assays, 50 nM NCPs were incubated with 500 nM BRCA1-f-BARD1²²¹ (W146Bpa or A195Bpa) with varying amounts of competitor 36-mer dsDNA or bubble-DNA (0, 0.3125, 0.625, 1.25, 2.5, 5, or 10 μ M) for 15 min at 4°C, and assays were performed as described above.

Cellular studies

Mammalian cell culture and transfection

HeLa cells (ATCC CCL-2) were grown in Dulbecco’s modified Eagles medium (DMEM) supplemented with 10% fetal bovine serum (Sigma), 100 μ g/ml streptomycin, and 100 U/ml penicillin (Sigma). The cells were tested for mycoplasma contamination by Bionique testing labs (<http://www.bionique.com/>). To create a FLP-in version of HeLa, we stably integrated a flippase recognition target (FRT) sequence into the cells by using the pFRT/lacZeo plasmid (Thermo Fisher Scientific). We tested Zeocin-resistant clones that had a single integration site detected by Southern blot for high-activity integration sites by using the mammalian b-galactosidase activity assay (Gal-Screen, Thermo Fisher Scientific). Clonal expansion of the selected colony established the HeLa-FRT cell line. To generate stable HeLa-FRT shBARD1 cells, Dharmacon™ TRIPZ™ lentiviral shRNAs against BARD1 (RHS4696) were transfected with their respective plasmids and individual clones were selected with 2 μ g/ml puromycin. To generate HeLa-FRT shBARD1 cell lines expressing HA-BARD1 WT or mutant (Δ 194–216), cells were transfected with their respective plasmids and individual clones were selected with 200 μ g/ml hygromycin. BARD1 was cloned into pcDNA5/FRT-HA vector. QuikChange site-directed mutagenesis was used to construct the mutant variant (Δ 194–216) of BARD1.

Immunoblot analysis

HeLa-shBARD1 cells stably expressing wild-type or Δ 194–216 mutant of HA-BARD1 were pretreated with doxycycline (1 μ g/ml) for 3 days to knockdown the endogenous BARD1, and then incubated with or without Olaparib (10 μ M) for another 24 h. Cells were trypsinized, and pellets were washed by PBS. Protein was extracted using NETN buffer (20 mM Tris-HCl pH 8, 420 mM NaCl, 1 mM EDTA, 0.5% IGEPAL, 1 mM DTT, and Roche Protease Inhibitor Cocktail) and were resolved in 8% Bis-Tris SDS-PAGE gels, and

blots (20–50 µg of total protein) were probed with the following antibodies: HA (3724S, Cell Signaling; 1:1,500), BRCA1 (SC6954, Santa Cruz; 1:500), BARD1 (ab50984, Abcam; 1:1,000), Tubulin (2128S, Cell Signaling; 1:2,000), Lamin B1 (SC374015, Santa Cruz, 1:500), according to the instructions provided by the manufacturers. The blots were incubated with HRP-conjugated secondary antibodies (Pierce 31450 for rabbit antimouse IgG-HRP; Sigma A6154 for goat antirabbit IgG-HRP) before being visualization of protein signals using the ECL max kit (Bio-rad).

Preparation of cytoplasmic and nuclear extracts

The REAP method for the preparation of cytoplasmic and nuclear extracts was followed. Briefly, HeLa cells from 10-cm dishes were washed with ice-cold phosphate buffer saline (PBS) pH 7.4, collected by centrifugation, resuspended in 900 µl of ice-cold PBS with 0.1% NP40 and protease inhibitors, and triturated 5 times using a p1000 micropipette. The lysed cell suspension was centrifuged for supernatant (this is the cytoplasmic fraction), and the pelleted nuclei was washed once with PBS with 0.1% NP40 and lysed by NETN buffer with protease inhibitors and different NaCl concentrations (100, 300, and 420 mM) to yield the nuclear extract fractions. Each soluble fraction was labeled as NS100, NS300, and NS420, while the final pellets were resuspended with NETN420 buffer and sonicated for 10 s for NP420 fraction. The cytoplasmic and nuclear fractions, 20 µg each, were analyzed by immunoblotting for their content of BRCA1, BARD1, Tubulin, and Lamin B1.

Immunofluorescence microscopy and image analysis

Cells were pretreated with doxycycline (1 µg/ml) for 3 days to knockdown the endogenous BARD1. Cells were trypsinized and 4×10^4 cells seeded in the 4-chambers slide with or without Olaparib (10 µM) for another 24 h. Cells were pre-extracted on ice for 10 min with cold cytoskeleton buffer (10 mM PIPES pH 6.8, 100 mM NaCl, 300 mM sucrose, 3 mM MgCl₂, 1 mM EGTA, 0.5% Triton X-100) followed by 10 min with cytoskeleton stripping buffer (10 mM Tris-HCl pH 7.4, 10 mM NaCl, 3 mM MgCl₂, 1% Tween 20 (v/v), 0.5% sodium deoxycholate). Pre-extracted cells were then fixed at room temperature for 10 min with 4% paraformaldehyde, washed with PBS, and treated for 10 min with 1% Triton X-100 in PBS. Primary anti-HA antibody (3724S, Cell Signaling; 1:500) was incubated overnight at 4°C in 5% goat serum in PBS. Alexa Fluor-568 conjugated secondary antibody (Jackson Immuno Research Labs) was incubated for 1 h at room temperature, and DAPI were incubated for another 15 min in room temperature. Then slides mounted using antifade mounting media (9071, Cell signaling). A random selection of 10–11 areas were imaged using an Evos M5000 Microscope. HA-BARD1 foci > 5 and HA-BARD1 foci per nuclear were quantified by the Celleste software and Prism GraphPad software was used for the final figure and significance analysis.

Clonogenic survival assay

HeLa cell lines stably expressing HA-BARD1 wild-type or mutant were pretreated with doxycycline for 3 days. Then, 400 cells/well were seeded into 12-well plates, treated with indicated amount of Olaparib (Selleckchem) or Cisplatin (Selleckchem) in regular growth medium for 11–12 days. Cells were fixed with methanol and stained with 0.5% crystal violet in methanol before colonies were counted.

Clonogenic survival was determined for a given concentration of cells that were plated by dividing the number of colonies on each treated plate by the number of colonies on the untreated plate, taking the plating efficiency of untreated cells into account.

Chemical cross-linking and mass spectrometry analysis

Sample preparation

Reactions were 90 µl of protein/nucleosome mix containing 2 mM BRCA1^{RING}/BARD1^{FL} and 2 mM of unmodified H2A or H2A K15-Ub nucleosomes wrapped with 147-bp “601” DNA in cross-linking buffer (25 mM HEPES-NaOH pH 7.5, 150 mM NaCl, 1% glycerol, 1 mM DTT) plus 3.06 µl of 14.5 mM DSS or BS3 (final concentration 0.5 mM) (DSS: disuccinimidyl suberate, BS3: bis(sulfosuccinimidyl)suberate, ThermoFisher). Cross-linking was carried out for 10, 30 or 45 min at room temperature before removing 30 µl and quenching by addition of 3 µl of 1 M ammonium bicarbonate at room temperature for 30 min. Four separate reaction conditions were performed: (i) WT-NCP DSS; (ii) WT-NCP BS3; (iii) K15Ub-NCP DSS; and (iv) K15Ub-NCP BS3. After quenching, 9 µl of each sample at each timepoint was analyzed by SDS-PAGE and the remainder was stored at –80°C until processing for mass spectrometry analysis.

Reactions were prepared for MS analysis by bringing them up to 0.1% PPS silent surfactant (Expedion Inc.), 5 mM TCEP. Samples were reduced for 60 min at 60°C in an Eppendorf Thermomixer with shaking (1,200 rpm). Alkylation was performed at room temperature in the dark for 30 min with 6 mM iodoacetamide. Excess iodoacetamide was quenched by addition of 5 mM DTT, and samples were then digested by trypsin digestion (Sequencing Grade Modified Trypsin, Promega Corp) at 37°C for 6 h in a Thermomixer with shaking (1,000 rpm) at a substrate to enzyme ratio of 15:1 prior to acidification with 250 mM HCl (final concentration). Acidified samples were incubated for 1 h at room temperature, spun at max speed in a microfuge and supernatants containing peptides were transferred to autosampler vials and stored at –80°C until analysis.

Chromatography

Mass spectrometry and data analysis were based on previously described methods (Zelter *et al*, 2015). For each injection, 3 µl of protein digests were loaded by autosampler onto a 150-µm Kasil fritted trap packed with 2 cm of Reprosil-Pur C18-AQ (3-µm bead diameter, Dr. Maisch) at a flow rate of 2.5 µl/min. After desalting with 8 µl of 0.1% formic acid plus 2% acetonitrile, the trap was brought online with a Self-Packed PicoFrit Column (New Objective part number PF360-75-10-N-5, 75 µm i.d.) packed with 30 cm of Reprosil-Pur C18-AQ (3-µm bead diameter, Dr. Maisch) mounted to a heated nanospray ionization source (CorSolutions LLC) set at 50°C and placed in line with a Thermo Scientific EASY-nLC 1200 UPLC pump plus autosampler.

Peptides were eluted from the column at 0.25 µl/min using an acetonitrile gradient consisting of the following steps: (i) 0–10 min; 6–10% B; (ii) 10–90 min; 10–32% B; (iii) 100–130 min; 32–75% B; (iv) 130–135 min; 75% B; (v) 135–136 min; 75–100% B; (vi) 136–151 min; 100% B, followed by re-equilibration to 0% buffer B prior to the subsequent injection. Buffer A was: 0.1% formic acid in water, and buffer B was 0.1% formic acid 80% acetonitrile.

Data acquisition

A Thermo Fisher Scientific Exploris 480 was used to perform mass spectrometry in positive ion mode with the following settings. Data-dependent acquisition (DDA) mode was used with a maximum of 20 tandem MS (MS/MS) spectra acquired per MS spectrum (scan range of m/z 400–1,600). The resolution for MS and MS/MS was 60,000 at m/z 200. The normalized automatic gain control targets for both MS and MS/MS were set to 100%, and the maximum injection times were 50 and 100 ms for MS and MS/MS scans, respectively. MS/MS spectra were acquired using an isolation width of 2 m/z and a normalized collision energy of 27. MS/MS acquisitions were prevented for +1, +2, $\geq +6$ or undefined precursor charge states. Dynamic exclusion was set for 10 s. MS and MS/MS spectra were collected in centroid mode.

MS data processing – identification of cross-linked peptides

Raw mass spectra were converted into mzML using ProteoWizard's msconvert (Chambers *et al.*, 2012). All proteins in the sample were identified using Comet (Eng *et al.*, 2013) searching against a database including the entire *S. frugiperda*, *E. coli*, and *H. sapiens* proteomes (Uniprot 7108, 83333 and 9606, respectively) plus common contaminants (<https://www.thegpm.org/crap/>) along with the sequences of all heterologously expressed proteins (FLAG-BRCA1, P38398; TwinStrepII-BARD1, Q99728; H2A-2A, Q99728; H2B-1K, O60814; H3.2 (C110A), Q71DI3; H4, P62805; Ub G76C, sequence derived from P0CG48). Smaller search databases were made for subsequent XL searching consisting only of proteins identified in initial comet searches by at least 3 peptides with a Percolator assigned q -value of ≤ 0.01 . Decoy databases consisted of the corresponding set of reversed protein sequences. Cross-linked peptides were identified within these proteins by Kojak version 2.0.0-alpha8 available at (<http://www.kojak-ms.org/>) (Hoopmann *et al.*, 2015). A statistically meaningful q -value was assigned to each peptide spectrum match (PSM) through analysis of the target and decoy PSM distributions using Percolator version 2.08 (Käll *et al.*, 2007). All data reported in this paper were filtered to show hits to the target proteins that had a Percolator assigned peptide level q value ≤ 0.05 .

NMR experiments and resonance assignments

All spectra were collected at 25°C in NMR buffer (25 mM MOPS-NaOH, 100 mM NaCl, 1 mM EDTA, and 0.5 mM TCEP, pH 7.0) with 7% D₂O. NMR HSQC and titration data were completed on a Bruker 800 MHz Avance III spectrometer with cryoprobe. (¹H,¹⁵N)-HSQC spectra were collected on the following ¹⁵N-BARD1 IDR constructs: BARD1 Ser-124-424, Ser-124-270, 269–424, and Ser-141-216.

(¹H,¹⁵N)- and (¹H,¹³C)-HSQC titration experiments were completed for BARD1 IDR + 36mer-dsDNA or 36mer-bubDNA by adding unlabeled DNA to 150 μ M [¹³C,¹⁵N]-BARD1 124–270 or 150 μ M [¹³C,¹⁵N]-BARD1 Ser-141-216, maintaining a constant concentration of the labeled species. Only apo and 1:1 spectra for the [¹³C,¹⁵N] BARD1 Ser-141-216 construct were obtained since intermediate titration points resulted in loss of sample. Additionally, titration spectra with nucleosome were collected for 150 μ M [¹³C,¹⁵N]-BARD1 124–270 + 0.05x NCP¹⁴⁷. A (¹H,¹⁵N)-HSQC was collected on 150 μ M ¹⁵N-BARD1 269–424 + 150 μ M 28mer-dsDNA.

Dynamics experiments were collected on a Bruker 500 MHz Avance III spectrometer with a room temperature probe. T₁ and T₂

¹⁵N-Trosy HSQC experiments for 150 μ M [¹³C,¹⁵N]-BARD1 Ser-141-216, 150 μ M [¹³C,¹⁵N]-BARD1 Ser-141-216 + 150 μ M 36mer-dsDNA, and 150 μ M [¹³C,¹⁵N]-BARD1 Ser-141-216 + 150 μ M 36mer-bubble-DNA were collected in an interleaved manner with 8 points each (Zhu *et al.*, 2000). T₁ delays were 10, 40, 80, 120, 160, 320, 640, and 1,000 ms; T₂ cpmg loop delays were 8.48, 16.96, 25.44, 25.44, 42.40, 50.88, 67.84, and 84.80 ms. T₁ and T₂ for each residue were fitted to a single exponential with errors reflecting the quality in the fit. Residues corresponding to peaks with overlapping intensities were excluded from the analysis.

Backbone chemical shift assignments were determined from standard backbone triple-resonance experiments (HNCA, HNCOCACB, HNCOCACB, HNCACB, HNCO, and HNCACO) and an HNHA experiment using a Bruker 800 MHz Avance III spectrometer with cryoprobe. The 3D data were collected for 500 μ M [¹³C,¹⁵N]-BARD1 Ser-124-270 and 500 μ M [¹³C,¹⁵N]-BARD1 Ser-141-216. Assignments from the shorter construct were transferred as appropriate to the longer BARD1 construct. HNCACB and HNCOCACB spectra were collected on the 1:1 samples of 150 μ M [¹³C,¹⁵N]-BARD1 Ser-141-216 with either 36mer dsDNA or 36mer bubble-DNA.

The NH chemical shift perturbation was calculated according to $\Delta\delta_{\text{NH}}$ (ppm) = $\sqrt{[\Delta\delta_{\text{H}}]^2 + (\Delta\delta_{\text{N}}/5)^2}$. Component ¹H and ¹⁵N chemical shift differences are (free – bound) in ppm. The CaCb CSP was calculated according to $\Delta\delta_{\text{CaCb}}$ (ppm) = $0.25 \times [(\text{C}\alpha\text{-C}\beta)_{\text{free}} - (\text{C}\alpha\text{-C}\beta)_{\text{bound}}]$. Secondary structure propensity (SSP) was determined from $\Delta\delta(\text{C}\alpha\text{-C}\beta) = (\text{C}\alpha\text{-C}\beta)_{\text{measured}} - (\text{C}\alpha\text{-C}\beta)_{\text{random coil}}$, where the random coil shifts were generated from BARD1 IDR sequence using a webserver (https://spin.niddk.nih.gov/bax/nmrserver/Poulsen_rc_CS/) (Kjaergaard & Poulsen, 2011).

Multiple sequence alignment

Mammalian BARD1 ortholog sequences were downloaded from Ensembl (v106), globally aligned using MAFFT (Katoh & Standley, 2013), and trimmed to BARD1 residues 124–270.

Data availability

Source data for H2A-Ub and binding assays as well as uncropped gels and blots and original microscopy images are included as supplemental files. For cross-linking mass-spectrometry analysis, the complete unfiltered list of all PSMs and their percolator assigned q values are available on the ProXL web application (Riffle *et al.*, 2016, 2019) <https://proxl.yeastrc.org/proxl/p/bard1nucleosome> along with the raw MS spectra and search parameters used. In addition, complete search algorithm configuration files, fasta search databases, raw search output, and raw MS data files were deposited to the ProteomeXchange Consortium via the PRIDE (Vizcaíno *et al.*, 2009) partner repository (<https://www.ebi.ac.uk/pride/archive>) with the dataset identifier PXD035345. NMR chemical shift assignments for BARD1 Ser-141-216 and associated DNA-bound assignments have been deposited to the Biological Magnetic Resonance Bank (<https://bmr.io>) with dataset identifiers 51523 (apo), 51524 (with dsDNA), 51525 (with bubble-DNA). Python scripts used to analyze and plot fluorescence-based binding data are included with this manuscript. Plasmid reagents generated in this study can be obtained upon request from the corresponding author Dr. Rachel Kleivit.

Expanded View for this article is available [online](#).

Acknowledgements

We thank K. Luger (University of Colorado Boulder) for sharing plasmids for the 147-bp and NLE-trimer “601” DNA, S. Tan (Penn State University) for sharing the plasmid for the 185-bp “601” DNA, and G. Debelouchina (UC San Diego) for the MMTV DNA plasmid. We thank D. Veelser for providing access to equipment, and M. Morgan for insights into dichloroacetone cross-linking of H2A-Ub. SRW, LMT, KEK, PSB, and REK were supported by the NIH (R01 CA260834). REK is the Edmond H. Fischer/Washington Research Foundation Endowed Chair in Biochemistry. This work and AZ was supported in part by the University of Washington’s Proteomics Resource (UWPR95794). AZ and TND were also supported by the NIH (P41 GM103533). WZ was supported by a Young Investigator Award from Max and Minnie Tomerlin Voelcker Fund, the Cancer Prevention and Research Institute of Texas (RP210102), and the NIH (R01 GM141091). DBW was supported by the NIH (R00-HD090201).

Author contributions

Rachel E Klevit: Conceptualization; data curation; formal analysis; supervision; funding acquisition; investigation; methodology; project administration; writing – review and editing. **Samuel R Witus:** Conceptualization; data curation; formal analysis; validation; investigation; visualization; methodology; writing – original draft; writing – review and editing. **Lisa M Tuttle:** Formal analysis; investigation; methodology; writing – review and editing. **Wenjing Li:** Investigation. **Alex Zelter:** Resources; investigation; methodology; writing – review and editing. **Meiling Wang:** Investigation. **Klaiten E Kermaode:** Investigation. **Damien B Wilburn:** Formal analysis; investigation; methodology; writing – review and editing. **Trisha N Davis:** Resources; supervision; writing – review and editing. **Peter S Brzovic:** Conceptualization; formal analysis; supervision; funding acquisition; writing – review and editing. **Weixing Zhao:** Conceptualization; formal analysis; supervision; writing – review and editing.

Disclosure and competing interests statement

The authors declare that they have no conflict of interest.

References

- Alenezi WM, Fierheller CT, Recio N, Tonin PN (2020) Literature review of BARD1 as a cancer predisposing gene with a focus on breast and ovarian cancers. *Genes* 11: 856
- Becker JR, Clifford G, Bonnet C, Groth A, Wilson MD, Chapman JR (2021) BARD1 reads H2A lysine 15 ubiquitination to direct homologous recombination. *Nature* 596: 433–437
- Belotserkovskaya R, Raga Gil E, Lawrence N, Butler R, Clifford G, Wilson MD, Jackson SP (2020) PALB2 chromatin recruitment restores homologous recombination in BRCA1-deficient cells depleted of 53BP1. *Nat Commun* 11: 819
- Sobhian B, Shao G, Lilli DR, Culhane AC, Moreau LA, Xia B, Livingston DM, Greenberg RA (2007) RAP80 targets BRCA1 to specific ubiquitin structures at DNA damage sites. *Science* 316: 1198–1202
- Bochar DA, Wang L, Beniya H, Kinev A, Xue Y, Lane WS, Wang W, Kashanchi F, Shiekhatter R (2000) BRCA1 is associated with a human SWI/SNF-related complex: linking chromatin remodeling to breast cancer. *Cell* 102: 257–265
- Brzovic PS, Rajagopal P, Hoyt DW, King MC, Klevit RE (2001) Structure of a BRCA1-BARD1 heterodimeric RING-RING complex. *Nat Struct Biol* 8: 833–837
- Brzovic PS, Keffe JR, Nishikawa H, Miyamoto K, Fox D, Fukuda M, Ohta T, Klevit R (2003) Binding and recognition in the assembly of an active BRCA1/BARD1 ubiquitin-ligase complex. *Proc Natl Acad Sci USA* 100: 5646–5651
- Chambers MC, Maclean B, Burke R, Amodei D, Ruderman DL, Neumann S, Gatto L, Fischer B, Pratt B, Egertson J et al (2012) A cross-platform toolkit for mass spectrometry and proteomics. *Nat Biotechnol* 30: 918–920
- Chin JW, Martin AB, King DS, Wang L, Schultz PG (2002) Addition of a photocrosslinking amino acid to the genetic code of *Escherichia coli*. *Proc Natl Acad Sci USA* 99: 11020–11024
- Christensen DE, Brzovic PS, Klevit RE (2007) E2-BRCA1 RING interactions dictate synthesis of mono- or specific polyubiquitin chain linkages. *Nat Struct Mol Biol* 14: 941–948
- Dai L, Dai Y, Han J, Huang Y, Wang L, Huang J, Zhou Z (2021) Structural insight into BRCA1-BARD1 complex recruitment to damaged chromatin. *Mol Cell* 81: 2765–2777
- Dao HT, Dul BE, Dann GP, Liszczak GP, Muir TW (2020) A basic motif anchoring ISWI to nucleosome acidic patch regulates nucleosome spacing. *Nat Chem Biol* 16: 134–142
- Davey NE (2019) The functional importance of structure in unstructured protein regions. *Curr Opin Struct Biol* 56: 155–163
- Densham RM, Morris JR (2019) Moving mountains—the BRCA1 promotion of DNA resection. *Front Mol Biosci* 6: 79
- Densham RM, Garvin AJ, Stone HR, Strachan J, Baldock RA, Daza-Martin M, Fletcher A, Blair-Reid S, Beesley J, Johal B et al (2016) Human BRCA1-BARD1 ubiquitin ligase activity counteracts chromatin barriers to DNA resection. *Nat Struct Mol Biol* 23: 647–655
- Dyer PN, Edayathumangalam RS, White CL, Bao Y, Chakravarthy S, Muthurajan UM, Luger K (2003) Reconstitution of nucleosome core particles from recombinant histones and DNA. In *Methods in Enzymology*, pp 23–44. Cambridge, MA: Academic Press
- Eng JK, Jahan TA, Hoopmann MR (2013) Comet: an open-source MS/MS sequence database search tool. *Proteomics* 13: 22–24
- Gudmundsdottir K, Ashworth A (2006) The roles of BRCA1 and BRCA2 and associated proteins in the maintenance of genomic stability. *Oncogene* 25: 5864–5874
- Hatchi E, Skourti-Stathaki K, Vents S, Pinello L, Yen A, Kamieniarz-Gdula K, Dimitrov S, Pathania S, McKinney KM, Eaton ML et al (2015) BRCA1 recruitment to transcriptional pause sites is required for R-loop-driven DNA damage repair. *Mol Cell* 57: 636–647
- Hoopmann MR, Zelter A, Johnson RS, Riffle M, MacCoss MJ, Davis TN, Moritz RL (2015) Kojak: efficient analysis of chemically cross-linked protein complexes. *J Proteome Res* 14: 2190–2198
- Hu Q, Botuyan MV, Zhao D, Cui G, Mer E, Mer G (2021) Mechanisms of BRCA1-BARD1 nucleosome recognition and ubiquitylation. *Nature* 596: 438–443
- Huen MSY, Sy SMH, Chen J (2010) BRCA1 and its toolbox for the maintenance of genome integrity. *Nat Rev Mol Cell Biol* 11: 138–148
- Kalb R, Mallery DL, Larkin C, Huang J, Hiom K (2014) BRCA1 is a histone-H2A-specific ubiquitin ligase. *Cell Rep* 8: 999–1005
- Käll L, Canterbury JD, Weston J, Noble WS, MacCoss MJ (2007) Semi-supervised learning for peptide identification from shotgun proteomics datasets. *Nat Methods* 4: 923–925
- Katoh K, Standley DM (2013) MAFFT multiple sequence alignment software version 7: improvements in performance and usability. *Mol Biol Evol* 30: 772–780
- Kjaergaard M, Poulsen FM (2011) Sequence correction of random coil chemical shifts: correlation between neighbor correction factors and changes in the Ramachandran distribution. *J Biomol NMR* 50: 157–165

- Kolas NK, Chapman JR, Nakada S, Ylanko J, Chahwan R, Sweeney FD, Panier S, Mendez M, Wildenhain J, Thomson TM *et al* (2007) Orchestration of the DNA-damage response by the RNF8 ubiquitin ligase. *Science* 318: 1637–1640
- Krais JJ, Johnson N (2020) BRCA1 mutations in cancer: coordinating deficiencies in homologous recombination with tumorigenesis. *Cancer Res* 80: 4601–4609
- Krais JJ, Wang Y, Patel P, Basu J, Bernhardt AJ, Johnson N (2021) RNF168-mediated localization of BARD1 recruits the BRCA1-PALB2 complex to DNA damage. *Nat Commun* 12: 5016
- Lazar GA, Desjarlais JR, Handel TM (1997) De novo design of the hydrophobic core of ubiquitin. *Protein Sci* 6: 1167–1178
- Lee Y-T, Gibbons G, Lee SY, Nikolovska-Coleska Z, Dou Y (2015) One-pot refolding of core histones from bacterial inclusion bodies allows rapid reconstitution of histone octamer. *Protein Expr Purif* 110: 89–94
- Lorick KL, Jensen JP, Fang S, Ong AM, Hatakeyama S, Weissman AM (1999) RING fingers mediate ubiquitin-conjugating enzyme (E2)-dependent ubiquitination. *Proc Natl Acad Sci USA* 96: 11364–11369
- Lowary PT, Widom J (1998) New DNA sequence rules for high affinity binding to histone octamer and sequence-directed nucleosome positioning. *J Mol Biol* 276: 19–42
- Luger K, Rechsteiner TJ, Richmond TJ (1999) Preparation of nucleosome core particle from recombinant histones. *Methods Enzymol* 304: 3–19
- Mark W-Y, Liao JCC, Lu Y, Ayed A, Laister R, Szymczynska B, Chakrabarty A, Arrowsmith CH (2005) Characterization of segments from the central region of BRCA1: an intrinsically disordered scaffold for multiple protein-protein and protein-DNA interactions? *J Mol Biol* 345: 275–287
- Masuda T, Xu X, Dimitriadis EK, Lahusen T, Deng C-X (2016) 'DNA binding region' of BRCA1 affects genetic stability through modulating the intra-S-phase checkpoint. *Int J Biol Sci* 12: 133–143
- Mattiroli F, Vissers JHA, van Dijk WJ, Ikpa P, Citterio E, Vermeulen W, Marteijn JA, Sixma TK (2012) RNF168 ubiquitinates K13-15 on H2A/H2AX to drive DNA damage signaling. *Cell* 150: 1182–1195
- McGinty RK, Henrici RC, Tan S (2014) Crystal structure of the PRC1 ubiquitylation module bound to the nucleosome. *Nature* 514: 591–596
- McGuffin LJ, Bryson K, Jones DT (2000) The PSIPRED protein structure prediction server. *Bioinformatics* 16: 404–405
- Morgan MT, Haj-Yahya M, Ringel AE, Bandi P, Brik A, Wolberger C (2016) Structural basis for histone H2B deubiquitination by the SAGA DUB module. *Science* 351: 725–728
- Morgan M, Jbara M, Brik A, Wolberger C (2019) Chapter one - Semisynthesis of ubiquitinated histone H2B with a native or nonhydrolyzable linkage. In *Methods in Enzymology*, Hochstrasser M (ed), pp 1–27. Cambridge, MA: Academic Press
- Mullan PB, Quinn JE, Harkin DP (2006) The role of BRCA1 in transcriptional regulation and cell cycle control. *Oncogene* 25: 5854–5863
- Nakamura K, Saredi G, Becker JR, Foster BM, Nguyen NV, Beyer TE, Cesa LC, Faull PA, Lukauskas S, Frimurer T *et al* (2019) H4K20me0 recognition by BRCA1-BARD1 directs homologous recombination to sister chromatids. *Nat Cell Biol* 21: 311–318
- Poepsel S, Kasinath V, Nogales E (2018) Cryo-EM structures of PRC2 simultaneously engaged with two functionally distinct nucleosomes. *Nat Struct Mol Biol* 25: 154–162
- Riffle M, Jaschob D, Zelter A, Davis TN (2016) ProXL (protein cross-linking database): a platform for analysis, visualization, and sharing of protein cross-linking mass spectrometry data. *J Proteome Res* 15: 2863–2870
- Riffle M, Jaschob D, Zelter A, Davis TN (2019) Proxl (protein cross-linking database): a public server, QC tools, and other major updates. *J Proteome Res* 18: 759–764
- Santos-Pereira JM, Aguilera A (2015) R loops: new modulators of genome dynamics and function. *Nat Rev Genet* 16: 583–597
- Savage KI, Harkin DP (2015) BRCA1, a 'complex' protein involved in the maintenance of genomic stability. *FEBS J* 282: 630–646
- Schlacher K, Wu H, Jasin M (2012) A distinct replication fork protection pathway connects Fanconi anemia tumor suppressors to RAD51-BRCA1/2. *Cancer Cell* 22: 106–116
- Scully R, Chen J, Ochs RL, Keegan K, Hoekstra M, Feunteun J, Livingston DM (1997) Dynamic changes of BRCA1 subnuclear location and phosphorylation state are initiated by DNA damage. *Cell* 90: 425–435
- Sherker A, Chaudhary N, Adam S, Heijink AM, Noordermeer SM, Fradet-Turcotte A, Durocher D (2021) Two redundant ubiquitin-dependent pathways of BRCA1 localization to DNA damage sites. *EMBO Rep* 22: e53679
- Simons AM, Horwitz AA, Starita LM, Griffin K, Williams RS, Glover JNM, Parvin JD (2006) BRCA1 DNA-binding activity is stimulated by BARD1. *Cancer Res* 66: 2012–2018
- Stewart MD, Zelin E, Dhall A, Walsh T, Upadhyay E, Corn JE, Chatterjee C, King M-C, Kleit RE (2018) BARD1 is necessary for ubiquitylation of nucleosomal histone H2A and for transcriptional regulation of estrogen metabolism genes. *Proc Natl Acad Sci USA* 115: 1316–1321
- Tan W, Murphy VJ, Charron A, van Twest S, Sharp M, Constantinou A, Parker MW, Crismani W, Bythell-Douglas R, Deans AJ (2020) Preparation and purification of mono-ubiquitinated proteins using Avi-tagged ubiquitin. *PLoS One* 15: e0229000
- Tarsounas M, Sung P (2020) The antitumorigenic roles of BRCA1-BARD1 in DNA repair and replication. *Nat Rev Mol Cell Biol* 21: 284–299
- Thapa I, Vahrenkamp R, Witus SR, Lightle C, Falkenberg O, Sellin Jeffries MK, Kleit RE, Stewart MD (2022) Conservation of transcriptional regulation by BRCA1 and BARD1 in *Caenorhabditis elegans*. *Nucleic Acids Res* 51: 2108–2116
- Uckelmann M, Densham RM, Baas R, Winterwerp HHK, Fish A, Sixma TK, Morris JR (2018) USP48 restrains resection by site-specific cleavage of the BRCA1 ubiquitin mark from H2A. *Nat Commun* 9: 229
- Virtanen P, Gommers R, Oliphant TE, Haberland M, Reddy T, Cournapeau D, Burovski E, Peterson P, Weckesser W, Bright J *et al* (2020) SciPy 1.0: fundamental algorithms for scientific computing in Python. *Nat Methods* 17: 261–272
- Vizcaíno JA, Côté R, Reisinger F, Foster JM, Mueller M, Rameseder J, Hermjakob H, Martens L (2009) A guide to the proteomics identifications database proteomics data repository. *Proteomics* 9: 4276–4283
- Wilkins MR, Gasteiger E, Bairoch A, Sanchez J-C, Williams KL, Appel RD, Hochstrasser DF (1999) Protein identification and analysis tools in the ExPASy server. In *2-D Proteome Analysis Protocols*, Link AJ (ed), pp 531–552. Totowa, NJ: Humana Press
- Wishart DS, Sykes BD, Richards FM (1991) Relationship between nuclear magnetic resonance chemical shift and protein secondary structure. *J Mol Biol* 222: 311–333
- Witus SR, Burrell AL, Farrell DP, Kang J, Wang M, Hansen JM, Pravat A, Tuttle LM, Stewart MD, Brzovic PS *et al* (2021a) BRCA1/BARD1 site-specific ubiquitylation of nucleosomal H2A is directed by BARD1. *Nat Struct Mol Biol* 28: 268–277
- Witus SR, Stewart MD, Kleit RE (2021b) The BRCA1/BARD1 ubiquitin ligase and its substrates. *Biochem J* 478: 3467–3483
- Witus SR, Zhao W, Brzovic PS, Kleit RE (2022) BRCA1/BARD1 is a nucleosome reader and writer. *Trends Biochem Sci* 47: 582–595
- Zelter A, Bonomi M, Kim JO, Umbreit NT, Hoopmann MR, Johnson R, Riffle M, Jaschob D, MacCoss MJ, Moritz RL *et al* (2015) The molecular architecture of the Dam1 kinetochore complex is defined by cross-linking based structural modelling. *Nat Commun* 6: 8673

- Zhao W, Steinfeld JB, Liang F, Chen X, Maranon DG, Jian Ma C, Kwon Y, Rao T, Wang W, Sheng C et al (2017) BRCA1-BARD1 promotes RAD51-mediated homologous DNA pairing. *Nature* 550: 360–365
- Zhu G, Xia Y, Nicholson LK, Sze KH (2000) Protein dynamics measurements by TROSY-based NMR experiments. *J Magn Reson* 143: 423–426
- Zhu Q, Pao GM, Huynh AM, Suh H, Tonnu N, Nederlof PM, Gage FH, Verma IM (2011) BRCA1 tumour suppression occurs via heterochromatin-mediated silencing. *Nature* 477: 179–184
- Zhu Q, Hoong N, Aslanian A, Hara T, Benner C, Heinz S, Miga KH, Ke E, Verma S, Soroczynski J et al (2018) Heterochromatin-encoded satellite RNAs induce breast cancer. *Mol Cell* 70: 842–853